

Modeling Sediment Accumulation and Soil Erosion with ^{137}Cs and ^{210}Pb in the Ala Wai Canal and Central Honolulu Watershed, Hawai'i¹

GARY M. MCMURTRY,² ANOND SNIDVONGS,^{2,3} AND CRAIG R. GLENN⁴

ABSTRACT: Radiochemical studies of sediments from the Ala Wai Canal, an urban estuary in Honolulu, and of soils and stream sediments from the central Honolulu watershed were undertaken to investigate the sediment accumulation history and estimate the sediment yield and denudation rate of the watershed. Modern high-purity Ge gamma spectrometry techniques were used to assess the activities of U-series and ^{137}Cs radioisotopes in stratigraphic subsamples of three 1- to 2-m-long sediment cores, 14 watershed soil horizons, and grab samples of seven tributary stream sediments. Geochronology based on excess ^{210}Pb , using either steady-state constant flux or constant activity models, yields ages that exceed the known age of the Ala Wai Canal. Geochronology based on a nonsteady-state, two-box, erosion/redeposition model of fallout ^{137}Cs yields sedimentation rates for the canal of between ca. 2 and 22 cm yr^{-1} . These rates generally exceed those based upon excess ^{210}Pb by more than a factor of two and agree with the known age of the canal and with sedimentation rate estimates based upon bathymetry changes. Based on the ^{137}Cs -model chronology from 1957 to 1991, the Ala Wai Canal collects bulk sediment at a mean rate of ca. 3100 tons annually. About 80% of the sediment is detrital clays from erosion of the central Honolulu watershed, whereas about 20% of the sediment is composed of marine authigenic and biogenous phases. The sediment yield for the central Honolulu watershed of ca. 60 metric tons $\text{km}^{-2} \text{yr}^{-1}$ equates to a physical denudation rate of ca. 6 $\text{mg cm}^{-2} \text{yr}^{-1}$ —at the low end of the range of physical denudation rate estimates for the island of O'ahu. Based on the mean ^{137}Cs sedimentation rates and an average canal water depth of 2 m, the average time to fill the canal is about 60 yr, assuming that little sediment escapes. The mean fill time is only about 40 yr for the middle canal segment, which receives most silt development from the Mānoa-Pālolo Stream drainage canal, whereas for the outer and inner canal sediments, mean fill times are about 70 yr. Fallout ^{137}Cs -derived sedimentation rates for each 4-cm interval range from <0.1 to $>1.0 \text{ g cm}^{-2} \text{ month}^{-1}$ and reveal three episodes of relatively high sediment accumulation in the canal over the ca. 35-yr period before 1991: 1957–1967, 1979–1982, and 1986–1991. The two earlier episodes appear to coincide with periods of high rainfall, but are generally preceded by dry periods where accumulation of marine authigenic phases are high. The most recent high sediment accumulation episode does not appear to correlate with high rainfall, although

¹University of Hawai'i School of Ocean and Earth Science and Technology contribution no. 3855 and University of Hawai'i Sea Grant contribution no. UNIHI-SEAGRANT JC-95-06. This study was funded in part by grants from the NOAA-UH Sea Grant College Program (R/ME-IPD) to G. M. McMurtry and E. H. De Carlo, and from the National Science Foundation University of Hawai'i Young Scholars Program (P. Fryer, Program Director).

²Department of Oceanography, School of Ocean and Earth Science and Technology, University of Hawai'i at Mānoa, Honolulu, Hawai'i 96822.

³Current address: Marine Science Department, Chulalongkorn University, Bangkok 10330 Thailand.

⁴Department of Geology and Geophysics, School of Ocean and Earth Science and Technology, University of Hawai'i at Mānoa, Honolulu, Hawai'i 96822.

the annual rainfall trend has increased toward 1990 from a low in 1983. For the Ala Wai Canal, the flux of excess ^{210}Pb generally follows the sedimentation rate and is not constant with time. Two possible causes of higher excess ^{210}Pb fluxes than those expected from a linear relationship are nonsteady-state atmospheric input to the Hawaiian Islands from ^{222}Rn -rich air masses that originate in Asia, and ^{222}Rn from local volcanic eruptions. The variable excess ^{210}Pb flux into the canal sediments may, however, be related to a complex mechanism of soil erosion.

THE ALA WAI CANAL is an elongate artificial estuary that was created in the 1920s to drain the wetlands area in Waikīkī for tourist resort development. Construction began on the canal in 1921 and was completed in 1927 (Glenn and McMurtry 1995). Freshwater discharge is received primarily from the convergence of the Mānoa and Pālolo Streams, which drain their respective valleys, and from Makiki Stream, whose valley flow was diverted into the canal. Freshwater is also received from runoff of the adjoining streets, from the Ala Wai Golf Course, and from natural springs located along the mauka (mountain) side of the canal (Figures 1 and 2). Seawater enters the canal from the Ala Wai Yacht Harbor and reaches all portions of the canal (Laws et al. 1993), despite a large sill that has developed at the mouth of the Mānoa-Pālolo Stream drainage canal. Sedimentation of the Ala Wai Canal from natural causes, perhaps amplified by the urbanization of Honolulu, has been a continuing problem for the city and county and manifests itself in this sill, which currently shoals at low tide in places near the mouth of the Mānoa-Pālolo drainage canal. The sill has been removed twice, once in 1966, and again in 1978, when a larger portion of the canal was dredged (Figure 2). The canal originally was dredged to an average depth of 3–6 m, but in 1971 the average depth was estimated to be no more than 2 m (Gonzalez 1971); today no portion of the canal is greater than 4 m deep (Laws et al. 1993). Restricted circulation within the canal promoted by the sedimentation has caused the bottom waters to become stratified, anoxic, and polluted, especially in the back portion of the canal (Glenn et al. 1995), whereas surface waters are hyper-eutrophic with conditions close to optimal for phytoplankton growth (Laws et al. 1993).

This study was initiated as part of a multidisciplinary program aimed at assessing the current and past status of the environmental quality of the Ala Wai Canal (Fryer 1995, Glenn and McMurtry 1995). Studies of the canal sedimentation were undertaken to complement many of these investigations by providing age constraints on the sediment accumulation so that historical records of the various sediment components could be made and the origins and causes of past hydrologic conditions and of the introduction of pollutants could be identified. The known age, small size, simple geometry, and known major sources of sediment introduction of the Ala Wai Canal make this estuarine system nearly ideal for the application and testing of sedimentation models. Together with historical records of rainfall and runoff, we also wished to use the modeling results to estimate erosion rates of the central Honolulu watershed (Makiki-Mānoa-Pālolo Valleys). To achieve these goals, we applied steady-state constant flux and constant activity models of excess ^{210}Pb activities to three Ala Wai Canal sediment cores and used the sediment core and watershed soil inventories of fallout ^{137}Cs activities in a nonsteady-state model to obtain sediment ages and an estimate of the average sediment yield from the central Honolulu watershed.

MATERIALS AND METHODS

The sediment cores were obtained in the summers of 1991 and 1992 by manually inserting plastic core-liners into the soft Ala Wai Canal sediments from a small boat positioned near the center of the canal at each coring site (Figures 1 and 2). After core recovery, sediment compaction upon coring

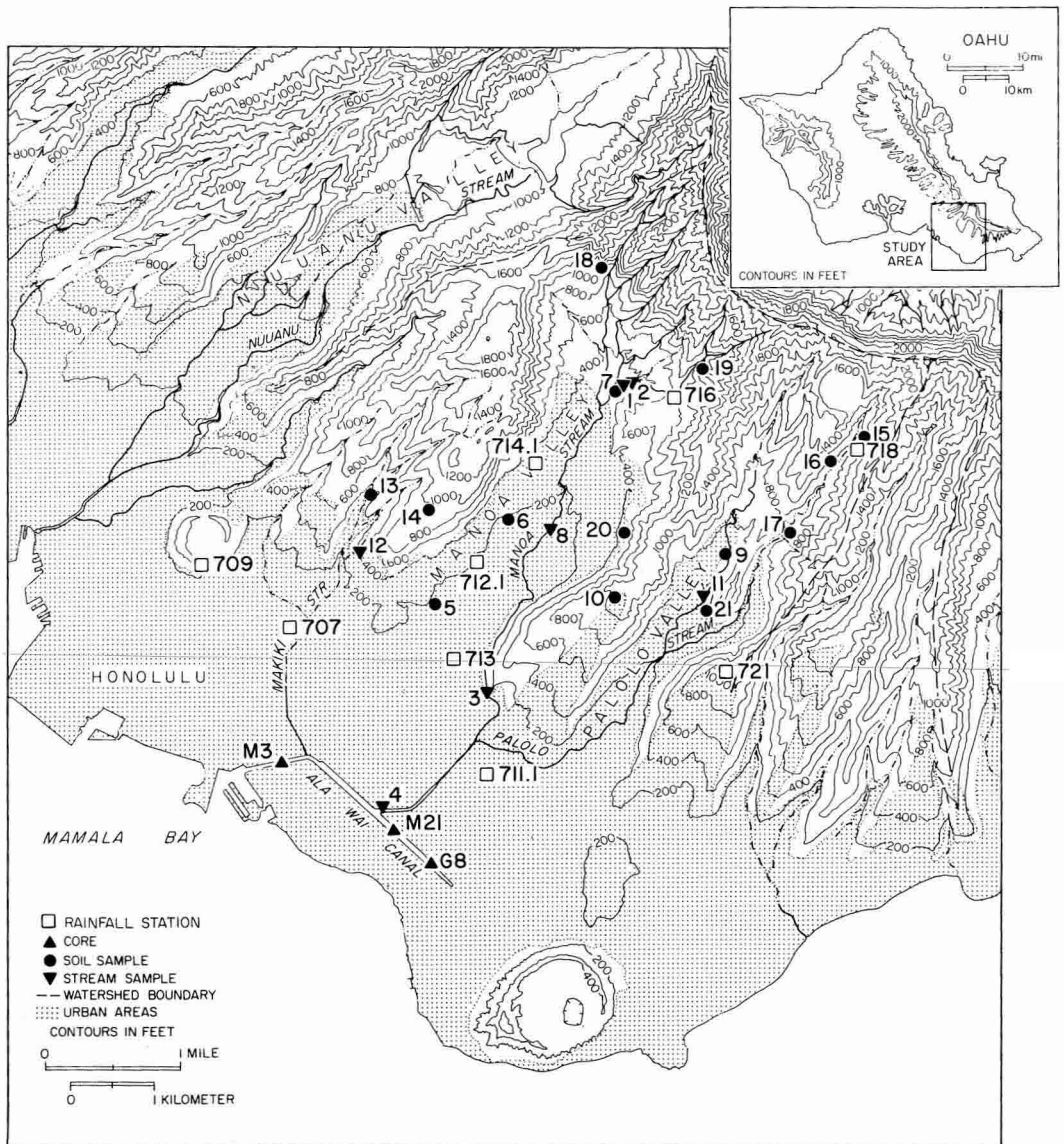


FIGURE 1. Topographic contour map of the central Honolulu watershed, consisting of the Makiki, Mānoa, and Pāloa Valleys and portions of the Honolulu coastal plain. Locations of Ala Wai Canal sediment cores, stream sediment and soil samples, and selected rainfall stations are indicated. Major streams are denoted by solid lines, minor streams by dash-dot lines, and watershed boundaries by dashed lines. Urban areas are indicated by shading. Inset: topographic contour map of O'ahu, Hawai'i, showing location of study area.

(estimated at less than 10%) was noted, excess water was drained from the liner headspace, and the cores were immediately transported in vertical position to our laboratories at the University of Hawai'i. The

cores were then frozen in vertical position, split into two halves with a table saw, and each thawed section visually described (cf. Glenn et al. 1995) and subsequently sampled. After thawing, each section was preserved in

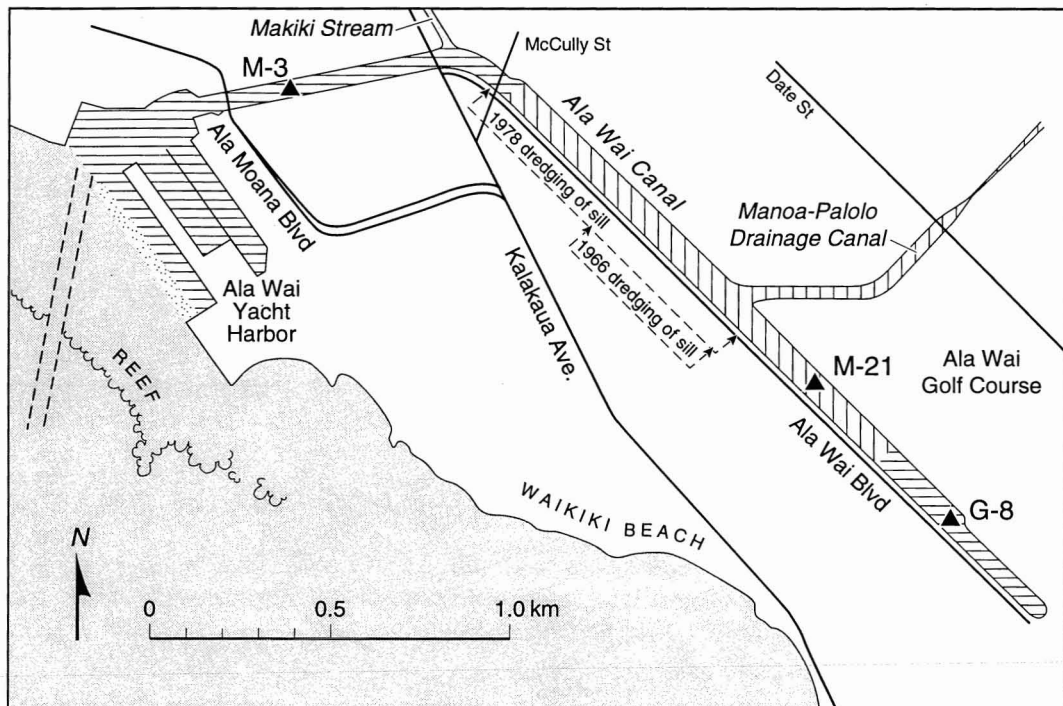


FIGURE 2. Location map of the Ala Wai Canal, showing three aerial sections (hatched) chosen to be represented by the three sediment cores studied (solid triangles). Areas affected by silt dredging in 1966 and 1978 are also indicated.

sealed plastic bags within plastic D-tubes and stored horizontally under refrigeration at 2°C. Of the numerous cores collected, this study focused on three cores recovered from areas of the canal that were unlikely to have been disturbed by dredging (Figure 2). Total recovered lengths for each core were 90 cm for Miller-3 (M-3), 164 cm for Miller-21 (M-21), and 200 cm for Gonzalez-8 (G-8). Water depths at these coring sites were 3.8, 3.0, and 3.1 m, respectively. For the radiochemical analysis, one-half of each core was subsampled at 4-cm intervals. Porosities and dry bulk densities were estimated for each sediment subsample by calculating the sectional volume sampled and measuring the sediment weight before and after oven drying for 48 hr at 110°C. Porosity determinations assumed complete porewater saturation.

Watershed soils and stream sediments were collected in 1991, 1992, and 1993. Sediment

grab samples were taken from the center of the stream at the site (Figure 1) and were wet sieved into two size fractions, 1000–45 μm and <45 μm , that were estimated by weight after oven drying for at least 24 hr at 60°C. Soil sample profiles from within the watershed were taken wherever possible away from urban development; however, a few sites were located near residences. The profiles were obtained by carefully hand digging 10-cm intervals to 50-cm depth and, in one case where an exposure was available, to 100-cm depth. Except as noted, soil dry bulk densities were measured by loosely packing moist samples into known volumes and oven drying for 48 hr at 110°C before weighing.

All samples for radiochemical analysis were dried at 110°C and ground with mortar and pestle. Weighed sample powders were sealed into plastic counting vials with high-vacuum resin and incubated for a minimum

TABLE 1
 SAMPLE DESCRIPTION: MĀNOA-PĀLOLO-MAKIKI VALLEYS WATERSHED AND ALA WAI CANAL

SAMPLE NO.	COLLECTION DATE	LOCATION	PHYSICAL DESCRIPTION AND COMMENTS	WEIGHT FRACTION (%)		AVG. DRY BULK DENSITY (g/cm ³)
				45–1000 μm	<45 μm	
NYS 92-1	23 June 1992	Mānoa Stream behind Paradise Park and near Lyon Arboretum	Gray-brown sandy gravel with silt and clay; collected in side tributary	76.5	23.5	—
NYS 92-2	23 June 1992	Mānoa Stream behind Paradise Park and near Lyon Arboretum	Gray-brown sandy gravel with silt and clay; collected in center of main streambed	89.2	10.8	—
NSY 92-3	23 June 1992	Mānoa Stream and Dole Street bridge	Gray-brown sandy gravel with silt and clay; collected in center of main streambed under bridge	39.7	60.3	—
NYS 92-4	23 June 1992	Mānoa and Pālolo Streams drainage into the Ala Wai Canal	Black sandy silt and clay with some gravel; hydrogen sulfide smell; collected on side of main stream	54.4	45.6	—
NYS 92-5	7 July 1992	Soil profile in Mānoa Valley at 2316 O'ahu Avenue	0–50 cm; dark brown changes to light brown at 20–25 cm; clumpy on top; finer grain size at depth; collected in front yard	—	—	1.20 ^a
NYS 92-6	14 July 1992	Soil profile in Mānoa Valley at 2654 Lowrey Avenue (corner lot)	0–50 cm; blackish brown at 0–50 cm to copper red and much additional moisture at bottom; collected in side yard near house	—	—	1.20 ^a
NYS 92-7	14 July 1992	Soil profile at Mānoa Stream on right bank by sample sites 92-1 and 92-2 when looking downstream	0–50 cm; brownish red, organic-rich soil; fine grain size; color changes to a lighter brown at 30–40 cm; minor basalt and Mn oxide-coated, altered rock fragments	—	—	0.80 ^a
NYS 92-8	14 July 1992	Mānoa Stream at Kahaloa Drive bridge	Gray-brown sandy gravel with silt and clay; collected in center of main streambed about 20 m downstream from bridge	92.4	7.6	—
NYS 92-9	16 July 1992	Soil profile in Pālolo Valley at 3160 Magnolia Drive (end of road)	0–50 cm; yellowish brown, rocky and dry soil; collected beneath large mango tree in side yard; site near bank of Pālolo Stream	—	—	0.92 ^a
NYS 92-10	16 July 1992	Soil profile on St. Louis Heights; Waahila Ridge State Recreation Area	0–50 cm; brownish red, organic-rich soil; red color intensifies with depth; collected in ironwood forest near entrance	—	—	0.84 ^a

NYS 92-11	16 July 1992	Pālolo Stream at Pukali Bridge	Gray-brown sandy gravel with silt and clay; collected in center of main streambed about 10 m upstream from bridge	89.3	10.7	—
NYS 92-12	24 July 1992	Makiki Stream; near corner of Round Top Drive and Makiki Street	Black sand with silt, clay and some gravel	92.4	7.6	—
NYS 92-13	24 July 1992	Soil profile in Makiki Forest Recreation Center	0–100 cm; red, moist, indurated clay; collected in road cut behind center and near active stream	—	—	0.97 ^a
NYS 92-14	24 July 1992	Soil profile in Tantalus Park	0–50 cm; blackish brown, organic-rich soil; collected in forested park near summit area	—	—	1.04 ^a
NYS 93-15	31 July 1993	Soil profile in Pālolo Valley; watershed reservation	0–50 cm; moist, dark brown, organic-rich soil; color change to brown at 30 cm; collected about 20 m above first falls in back of Pālolo Valley	—	—	0.68 ± 0.11 (n = 5)
NYS 93-16	31 July 1993	Soil profile in Pālolo Valley; watershed reservation	0–50 cm; moist brown soil; color change to reddish brown at 30 cm; collected about 500 m downstream from 93-15 site, on ~30° slope about 5 m above trail	—	—	0.65 ± 0.03 (n = 5)
NYS 93-17	31 July 1993	Soil profile in Pālolo Valley; watershed reservation	0–50 cm; brown, organic-rich soil; sharp color change to brownish red at 30 cm; collected about 20 m off trail under large eucalyptus trees near entrance and pump station	—	—	0.68 ± 0.05 (n = 5)
NYS 93-18	9 August 1993	Soil profile in Mānoa Valley at Mānoa Falls	0–60 cm; moist reddish brown clay; color change to brown at 40 cm; collected in trail cut about 200 m downstream from Mānoa Falls	—	—	0.66 ± 0.08 (n = 6)
NYS 93-19	9 August 1993	Soil profile in Mānoa Valley at Mānoa Tunnel no. 2	0–50 cm; moist, dark brown, organic-rich soil; color change to brown at 30 cm; collected in trail cut about 20 m downstream from Mānoa Tunnel no. 2	—	—	0.63 ± 0.08 (n = 5)
NYS 93-20	9 August 1993	Soil profile in Mānoa Valley at 3119 Beaumont Woods Place	0–50 cm; brown, organic-rich soil; collected in side yard near large outcropping of boulders and under large ironwood trees	—	—	0.85 ± 0.07 (n = 5)
NYS 93-21	9 August 1993	Soil profile in Pālolo Valley at Pālolo Chinese Home	0–50 cm; dark brown, organic-rich soil; collected about 20 m up on slope behind home complex about 50 m from entrance, in natural forest area	—	—	0.84 ± 0.04 (n = 5)

TABLE 1 (continued)

SAMPLE NO.	COLLECTION DATE	LOCATION	PHYSICAL DESCRIPTION AND COMMENTS	WEIGHT FRACTION (%) 45–1000 μm	AVG. DRY BULK DENSITY (g/cm ³)
Miller-3	11 July 1991	Ala Wai Canal, in center of canal near intersection of Ala Wai Boulevard and Lipe'epe'e Street	0–90 cm; dusky yellowish brown mud; collected in 3.8 m water depth	—	0.52 \pm 0.11 (n = 23)
Miller-21	9 July 1991	Ala Wai Canal, in center of canal between intersection of Ala Wai Boulevard with Seaside Avenue and Nohonani Street	0–164 cm; grayish black mud; some intercalated gray-white layers between 135 and 150 cm; collected in 3.0 m water depth	—	0.36 \pm 0.07 (n = 41)
Gonzalez-8	9 July 1991	Ala Wai Canal, in center of canal near intersection of Ala Wai Boulevard and 'Ohua Avenue	0–200 cm; grayish black mud; some intercalated gray layers at 30–50 cm with change to gray carbonate-rich mud at 162 cm; collected in 3.1 m water depth	—	0.29 \pm 0.10 (n = 50)

^aMaximum values based on previously dried samples, 0- to 10-cm intervals only.

of 3 weeks to allow ingrowth of ²²²Rn and daughter activities before counting. Uranium-series and ¹³⁷Cs radionuclide activities were determined simultaneously by non-destructive gamma spectrometry using an extended-range, coaxial, high-purity Ge detector (EG&G Ortec Gamma-X) with spectrum acquisition on a 4096-channel multi-channel analyzer. Samples were corrected for geometry and for self-absorption of ²¹⁰Pb and ²³⁴Th activities after methods previously described (Kim and Burnett 1983, Kim and McMurtry 1991). Spectral data were subsequently manipulated by computer and the reported net specific activities, normalized to NBS and EPA standards, were decay-corrected to the date of sample collection. Excess ²¹⁰Pb and ²²⁶Ra activities are reported as the difference between total ²¹⁰Pb and ²²⁶Ra activities and between total ²²⁶Ra and ²³⁴Th (²³⁸U) activities, respectively, assuming all ²³⁴Th activities are in secular equilibrium with ²³⁸U.

A detrital fraction of the Ala Wai Canal sediments was calculated as $DF (\%) = [1 - (\text{CaCO}_3 + \text{C}_{\text{org}} + \text{S})] \cdot 100$, using concentrations of CaCO₃, C_{org}, and S from Glenn et al. (1995). These detrital fractions are probably maximum values because abundant diatom tests and other biosiliceous material noted in these cores (Glenn et al. 1995, Resig et al. 1995) were not included in the calculations. The mean Si/Al ratio of the canal sediment cores (M-3, M-21, G-8B) of 1.57 ± 0.12 is only slightly higher than the mean Si/Al ratio of the <45- μm fraction of three Mānoa Stream sediment samples (1.23 ± 0.27 [De Carlo and Spencer 1995]) that likely represent nearly pure detrital material from watershed soil erosion. The abundance of biosiliceous material in the Ala Wai Canal sediments therefore does not appear substantial relative to the other components.

RESULTS AND DISCUSSION

The sediments of the Ala Wai Canal are dark brown to black anoxic muds primarily composed of detrital clays (smectite and chlorite) with admixtures of microcrystalline

TABLE 2

MILLER-3 CORE: URANIUM- AND THORIUM-SERIES RADIONUCLIDE AND FALLOUT ^{137}Cs ACTIVITIES

DEPTH INTERVAL (cm)	DRY BULK DENSITY (g/cm ³)	DETRITAL FRACTION (%) ^a	^{210}Pb		Ex. ^{210}Pb		^{226}Ra (pCi/g)	^{238}U		^{232}Th		^{137}Cs		
			(pCi/g)	+/-	(pCi/g)	+/-		+/-	(pCi/g)	+/-	(pCi/g)	+/-	(pCi/g)	+/-
0-4	0.346	86.9	4.36	0.14	4.06	0.14	0.303	0.010	0.971	0.088	0.500	0.018	0.421	0.016
4-8	0.269	84.6	4.20	0.17	3.92	0.17	0.281	0.012	0.951	0.088	0.638	0.025	0.471	0.021
8-12	0.337	79.3	3.42	0.15	3.09	0.15	0.333	0.011	0.910	0.093	0.470	0.017	0.403	0.018
12-16	0.425	80.5	3.03	0.13	2.73	0.13	0.304	0.009	0.943	0.081	0.560	0.018	0.385	0.015
16-20	0.509	86.2	2.84	0.12	2.58	0.12	0.260	0.008	1.093	0.078	0.500	0.016	0.291	0.012
20-24	0.613	79.9	1.95	0.11	1.66	0.11	0.296	0.008	1.173	0.058	0.472	0.014	0.364	0.013
24-28	0.618	86.7	1.18	0.08	0.87	0.08	0.314	0.007	1.082	0.063	0.544	0.012	0.436	0.011
28-32	0.633	86.8	0.81	0.08	0.51	0.08	0.301	0.006	0.780	0.045	0.639	0.012	0.609	0.013
32-36	0.533	89.8	1.28	0.08	0.96	0.08	0.316	0.006	1.073	0.060	0.709	0.013	0.759	0.014
36-40	0.699	89.0	1.15	0.08	0.87	0.08	0.274	0.007	1.040	0.065	0.437	0.011	0.463	0.012
40-44	0.635	84.0	1.13	0.10	0.81	0.10	0.318	0.009	0.775	0.058	0.613	0.015	0.729	0.019
44-48	0.466	83.8	0.50	0.10	0.22	0.10	0.286	0.009	1.200	0.084	0.763	0.017	1.000	0.022
48-52	0.506	86.1	0.74	0.08	0.44	0.08	0.309	0.007	0.739	0.063	0.852	0.017	0.673	0.015
52-56	0.515	83.4	1.16	0.09	0.84	0.09	0.323	0.007	1.154	0.068	0.580	0.014	0.476	0.013
56-60	0.520	83.2	0.64	0.10	0.34	0.10	0.300	0.008	0.883	0.078	0.588	0.016	0.497	0.016
60-64	0.647	80.7	0.82	0.09	0.53	0.10	0.289	0.008	1.160	0.079	0.707	0.018	0.649	0.017
64-68	0.529	85.6	0.47	0.09	0.17	0.09	0.303	0.007	1.901	0.092	0.598	0.018	0.241	0.011
68-72	0.604	78.4	1.10	0.09	0.67	0.09	0.433	0.008	1.190	0.071	0.606	0.015	0.163	0.008
72-76	0.594	65.3	0.91	0.08	0.72	0.09	0.189	0.006	1.263	0.068	0.446	0.015	0.084	0.007
76-80	0.581	72.6	0.64	0.11	0.36	0.11	0.283	0.010	1.704	0.097	0.537	0.021	0.030	0.007
80-84	0.575	81.2	0.70	0.10	0.33	0.10	0.366	0.009	1.582	0.088	0.367	0.015	0.040	0.007
84-87	0.362	90.5	0.80	0.11	0.48	0.11	0.318	0.010	1.525	0.095	0.362	0.017	0.030	0.007
87-90	0.443	85.1	0.83	0.10	0.39	0.10	0.435	0.010	1.385	0.067	0.663	0.021	0.018	0.006

Errors based on counting statistics ($\pm 1\sigma$)^aDetrital Fraction (%) = $[1 - (\text{CaCO}_3 + C_{\text{org}} + \text{S})] \cdot 100$. Concentrations of CaCO_3 , C_{org} , and S from Glenn et al. (1995).

TABLE 3

MILLER-21 CORE: URANIUM- AND THORIUM-SERIES RADIONUCLIDE AND FALLOUT ^{137}Cs ACTIVITIES

DEPTH INTERVAL (cm)	DRY BULK DENSITY (g/cm ³)	DETRITAL FRACTION (%) ^a	^{210}Pb		Ex. ^{210}Pb		^{226}Ra		^{238}U		^{232}Th		^{137}Cs	
			(pCi/g)	+/-	(pCi/g)	+/-	(pCi/g)	+/-	(pCi/g)	+/-	(pCi/g)	+/-	(pCi/g)	+/-
0-4	0.283	85.3	3.19	0.12	2.85	0.12	0.337	0.011	0.850	0.067	0.471	0.016	0.460	0.016
4-8	0.273	82.5	3.57	0.16	3.24	0.16	0.331	0.014	0.883	0.108	0.486	0.022	0.461	0.021
8-12	0.258	85.0	3.49	0.15	2.92	0.15	0.573	0.016	0.578	0.098	0.755	0.023	0.595	0.023
12-16	0.219	89.1	3.59	0.17	3.19	0.17	0.399	0.016	0.632	0.110	0.677	0.026	0.626	0.025
16-20	0.289	86.5	4.03	0.16	3.68	0.16	0.352	0.013	1.310	0.107	0.528	0.019	0.616	0.022
20-24	0.284	87.1	4.10	0.16	3.84	0.16	0.262	0.012	0.804	0.098	0.484	0.019	0.555	0.021
24-28	0.242	86.1	3.30	0.15	3.13	0.16	0.167	0.011	0.654	0.083	0.350	0.012	0.583	0.023
28-32	0.277	85.4	3.82	0.15	3.46	0.16	0.363	0.011	0.541	0.095	0.478	0.019	0.510	0.020
32-36	0.298	84.9	3.62	0.15	3.34	0.15	0.282	0.011	0.468	0.089	0.510	0.019	0.582	0.021
36-40	0.335	82.0	3.56	0.14	3.34	0.14	0.223	0.009	0.865	0.072	0.454	0.017	0.645	0.021
40-44	0.330	82.0	3.05	0.13	2.75	0.13	0.307	0.011	0.834	0.091	0.600	0.020	0.624	0.020
44-48	0.375	81.8	3.05	0.13	2.70	0.13	0.352	0.011	0.966	0.088	0.536	0.017	0.706	0.021
48-52	0.373	85.7	2.72	0.09	2.47	0.09	0.254	0.006	0.675	0.059	0.596	0.013	0.630	0.013
52-56	0.373	84.5	2.20	0.11	1.88	0.11	0.319	0.009	1.189	0.063	0.681	0.017	0.738	0.018
56-60	0.382	83.1	2.20	0.12	1.91	0.12	0.287	0.010	1.298	0.091	0.533	0.017	0.734	0.021
60-64	0.314	84.5	2.59	0.14	2.22	0.14	0.370	0.012	1.427	0.104	0.741	0.023	0.822	0.024
64-68	0.304	85.0	2.35	0.11	2.04	0.11	0.307	0.009	0.984	0.065	0.755	0.019	0.863	0.020
68-72	0.317	85.9	1.99	0.11	1.73	0.11	0.264	0.009	0.653	0.080	0.662	0.018	0.779	0.020
72-76	0.279	85.8	1.32	0.13	1.03	0.13	0.294	0.012	0.679	0.097	0.619	0.022	0.785	0.025
76-80	0.318	88.9	1.72	0.12	1.47	0.12	0.248	0.010	0.843	0.094	0.836	0.024	0.977	0.026
80-84	0.335	88.2	1.35	0.10	1.10	0.10	0.245	0.008	0.327	0.072	0.571	0.016	0.795	0.019
84-88	0.373	87.3	1.04	0.11	0.75	0.11	0.282	0.009	0.667	0.085	0.736	0.023	0.634	0.020
88-92	0.374	88.1	0.81	0.09	0.50	0.09	0.309	0.008	0.947	0.075	0.538	0.015	0.550	0.016
92-96	0.380	88.0	0.88	0.09	0.63	0.09	0.250	0.008	0.727	0.057	0.511	0.015	0.579	0.016
96-100	0.400	86.7	0.97	0.09	0.66	0.09	0.305	0.008	0.571	0.056	0.582	0.015	0.658	0.017
100-104	0.403	86.9	0.69	0.10	0.45	0.10	0.240	0.009	0.659	0.082	0.517	0.017	0.592	0.019
104-108	0.404	86.1	0.65	0.10	0.40	0.10	0.245	0.008	0.620	0.080	0.591	0.019	0.595	0.019
108-112	0.392	91.1	0.94	0.09	0.65	0.09	0.294	0.007	0.350	0.053	0.776	0.017	0.945	0.019
112-116	0.422	92.3	0.51	0.10	0.19	0.10	0.314	0.009	0.227	0.073	0.713	0.018	0.908	0.022

TABLE 3 (continued)

DEPTH INTERVAL (cm)	DRY BULK DENSITY (g/cm ³)	DETRITAL FRACTION (%) ^a	²¹⁰ Pb (pCi/g)	+/-	Ex. ²¹⁰ Pb (pCi/g)	+/-	²²⁶ Ra (pCi/g)	+/-	²³⁸ U (pCi/g)	+/-	²³² Th (pCi/g)	+/-	¹³⁷ Cs (pCi/g)	+/-
116-120	0.459	93.9	0.96	0.09	0.71	0.07	0.251	0.064	0.367	0.064	0.739	0.015	0.969	0.018
120-124	0.399	90.3	0.92	0.11	0.69	0.009	0.234	0.080	0.651	0.080	0.756	0.018	1.163	0.025
124-128	0.455	81.7	0.99	0.11	0.77	0.008	0.219	0.065	0.991	0.065	0.827	0.019	1.144	0.025
128-132	0.416	88.0	0.99	0.11	0.76	0.008	0.223	0.077	0.429	0.077	0.836	0.019	1.290	0.016
132-136	0.435	72.9	0.63	0.10	0.40	0.007	0.223	0.087	1.341	0.087	0.644	0.018	0.826	0.021
136-140	0.543	56.7	0.50	0.09	0.27	0.007	0.227	0.087	2.427	0.087	0.507	0.014	0.559	0.015
140-144	0.486	81.7	0.40	0.10	0.13	0.009	0.275	0.086	1.219	0.086	0.646	0.018	0.737	0.020
144-148	0.414	89.9	0.94	0.10	0.65	0.007	0.290	0.074	0.621	0.074	0.796	0.019	1.044	0.023
148-152	0.353	90.3	0.82	0.11	0.56	0.009	0.259	0.068	0.763	0.068	0.532	0.019	0.564	0.019
152-156	0.407	90.3	0.43	0.10	0.11	0.005	0.320	0.077	0.490	0.077	0.555	0.018	0.460	0.017
156-160	0.384	90.6	0.83	0.11	0.57	0.009	0.267	0.073	0.199	0.073	0.322	0.015	0.284	0.014
160-164	0.441	91.7	0.62	0.08	0.29	0.008	0.326	0.068	0.742	0.068	0.589	0.016	0.285	0.011

Errors based on counting statistics ($\pm 1\sigma$)

^aDetrital Fraction (%) = $[1 - (\text{CaCO}_3 + C_{\text{org}} + S)] \cdot 100$. Concentrations of CaCO₃, C_{org}, and S from Glenn et al. (1995).

carbonate muds that appear gray with increasing proportions. In addition to the predominant detrital components, the canal sediments have relatively high organic carbon contents of mixed marine/terrestrial origin (ca. 1–8%), authigenic calcium carbonate of abiotic origin (ca. 6–68%), and abundant diatom tests and pyrite (Glenn et al. 1995). Infauna are scarce to nonexistent (Resig et al. 1995); bioturbation effects are therefore considered negligible, although no fine laminations or sediment varving were evident (Glenn et al. 1995). Sample descriptions for the sediments and soils are presented in Table 1 with estimates of soil dry bulk densities. The activities of total ²¹⁰Pb, excess ²¹⁰Pb, total ²²⁶Ra, excess ²²⁶Ra, ²³⁸U, ²³²Th, and ¹³⁷Cs along with dry bulk densities for each sample interval of cores M-3, M-21, and G-8 are presented in Tables 2, 3, and 4. Table 5 presents the activities of total ²¹⁰Pb, excess ²¹⁰Pb, total ²²⁶Ra, excess ²²⁶Ra, ²³⁸U, ²³²Th, and ¹³⁷Cs for the central Honolulu watershed soils and stream sediments.

The distribution of sediment porosity with depth for cores M-3, M-21, and G-8 is presented in Figure 3. For cores G-8 and M-21, porosities generally decrease uniformly, with low values representing fine-grained, carbonate-rich sediment layers (Glenn et al. 1995). These variations may reflect sediment compaction, but are also correlated with decreases in organic carbon with depth (Glenn et al. 1995). Core M-3 displays a much steeper porosity gradient in its upper portion and low values in deeper sections that do not correlate with carbonate-rich sediment layers. For this core, porosity appears dominated by organic carbon variations with depth (Glenn et al. 1995).

The downcore distributions of ²³⁸U, ²²⁶Ra, and ²³²Th activities are presented in Figure 4. Activity variations of ²³⁸U are primarily correlated with those of authigenic calcium carbonate, with the highest ²³⁸U concentrations occurring in the back-basin core G-8. Seawater ²³⁸U is apparently scavenged from the canal into or onto authigenic calcium carbonate under anoxic conditions. The origin of the calcium carbonate in these sediments and correlation with ²³⁸U activi-

TABLE 4

GONZALEZ-8 CORE: URANIUM- AND THORIUM-SERIES RADIONUCLIDE AND FALLOUT ^{137}Cs ACTIVITIES

DEPTH INTERVAL (cm)	DRY BULK DENSITY (g/cm ³)	DETRITAL FRACTION (%) ^a	^{210}Pb		Ex. ^{210}Pb		^{226}Ra		^{238}U		^{232}Th		^{137}Cs	
			(pCi/g)	+/-	(pCi/g)	+/-	(pCi/g)	+/-	(pCi/g)	+/-	(pCi/g)	+/-	(pCi/g)	+/-
0-4	0.117	83.5	3.64	0.26	3.30	0.27	0.332	0.023	1.222	0.204	0.425	0.038	0.449	0.034
4-8	0.209	82.1	3.69	0.15	3.19	0.16	0.495	0.016	0.589	0.086	0.631	0.022	0.526	0.022
8-12	0.198	83.3	3.09	0.16	2.36	0.16	0.732	0.020	1.136	0.128	0.734	0.021	0.517	0.023
12-16	0.215	82.5	2.65	0.15	1.93	0.15	0.715	0.020	1.168	0.095	0.776	0.020	0.513	0.023
16-20	0.245	80.5	2.75	0.14	2.17	0.15	0.581	0.017	0.652	0.085	0.573	0.012	0.481	0.021
20-24	0.201	79.8	1.33	0.11	1.06	0.11	0.279	0.011	0.775	0.091	0.526	0.022	0.418	0.018
24-28	0.222	74.1	2.36	0.13	1.90	0.13	0.461	0.014	1.345	0.106	0.710	0.022	0.520	0.019
28-32	0.213	62.6	1.30	0.13	0.94	0.14	0.356	0.014	1.603	0.123	0.486	0.023	0.423	0.021
32-36	0.179	77.5	1.19	0.16	0.91	0.16	0.276	0.016	2.181	0.152	0.586	0.026	0.564	0.027
36-40	0.177	74.0	1.02	0.12	0.81	0.12	0.208	0.011	2.976	0.127	0.456	0.018	0.532	0.020
40-44	0.180	82.3	1.47	0.15	1.13	0.16	0.334	0.014	2.143	0.152	0.781	0.034	0.596	0.028
44-48	0.222	61.9	1.20	0.13	0.93	0.13	0.270	0.012	2.982	0.125	0.447	0.024	0.368	0.020
48-52	0.223	70.2	1.13	0.13	0.88	0.13	0.252	0.009	4.247	0.132	0.465	0.016	0.407	0.014
52-56	0.240	84.3	1.06	0.10	0.64	0.10	0.421	0.011	1.358	0.093	0.834	0.021	0.879	0.022
56-60	0.199	87.8	0.88	0.12	0.43	0.12	0.441	0.014	1.429	0.096	0.973	0.026	1.496	0.037
60-64	0.227	86.3	0.69	0.12	0.40	0.12	0.291	0.012	0.966	0.107	1.045	0.027	1.483	0.035
64-68	0.238	87.3	1.06	0.11	0.77	0.11	0.294	0.011	0.782	0.094	0.702	0.020	0.926	0.026
68-72	0.248	87.8	1.09	0.10	0.67	0.10	0.425	0.011	1.124	0.087	0.698	0.020	0.481	0.017
72-76	0.205	86.8	0.87	0.12	0.42	0.12	0.453	0.014	1.144	0.113	0.851	0.030	0.481	0.022
76-80	0.266	87.5	0.69	0.09	0.24	0.09	0.454	0.011	0.665	0.079	0.607	0.018	0.319	0.014
80-84	0.240	88.4	0.75	0.11	0.43	0.11	0.325	0.011	1.115	0.082	0.563	0.024	0.223	0.015
84-88	0.290	88.2	0.70	0.09	0.27	0.09	0.429	0.011	1.012	0.084	0.576	0.019	0.191	0.012
88-92	0.289	86.2	0.76	0.10	0.40	0.11	0.358	0.010	1.056	0.073	0.661	0.025	0.067	0.009
92-96	0.256	85.6	0.65	0.11	0.16	0.11	0.491	0.013	1.052	0.101	0.604	0.024	0.038	0.009
96-100	0.284	88.8	0.57	0.10	0.15	0.10	0.423	0.011	0.789	0.089	0.624	0.023	0.019	0.008
100-104	0.288	87.0	0.76	0.10	0.32	0.10	0.437	0.012	0.715	0.070	0.523	0.021	0.039	0.009
104-108	0.290	85.4	0.50	0.09	0.14	0.09	0.360	0.008	0.889	0.060	0.411	0.016	0.010	0.006
108-112	0.270	81.8	0.66	0.08	0.30	0.08	0.363	0.009	1.157	0.059	0.431	0.015	n.d.	n.d.
112-116	0.260	80.0	0.77	0.11	0.34	0.11	0.425	0.013	1.232	0.085	0.511	0.023	0.023	0.009
116-120	0.277	79.1	0.67	0.11	0.30	0.11	0.367	0.011	1.367	0.077	0.404	0.019	n.d.	n.d.
120-124	0.284	81.8	0.81	0.11	0.38	0.11	0.424	0.011	1.177	0.077	0.632	0.025	n.d.	n.d.
124-128	0.242	71.0	0.78	0.09	0.54	0.09	0.240	0.009	2.856	0.094	0.292	0.015	n.d.	n.d.
128-132	0.255	77.3	1.03	0.12	0.72	0.12	0.302	0.011	2.358	0.089	0.385	0.021	n.d.	n.d.
132-136	0.318	81.8	0.52	0.09	0.19	0.10	0.328	0.010	1.624	0.074	0.328	0.017	n.d.	n.d.
136-140	0.338	82.9	0.48	0.08	0.21	0.08	0.271	0.008	1.616	0.080	0.297	0.014	n.d.	n.d.
140-144	0.397	88.9	0.48	0.09	0.21	0.09	0.270	0.009	1.375	0.068	0.342	0.016	0.014	0.006
144-148	0.329	86.7	0.56	0.08	0.24	0.08	0.320	0.008	1.202	0.077	0.395	0.015	0.003	0.005

TABLE 4 (continued)

DEPTH INTERVAL (cm)	DRY BULK DENSITY (g/cm ³)	DETRITAL FRACTION (%) ^a	²¹⁰ Pb (pCi/g)	+/-	Ex. ²¹⁰ Pb (pCi/g)	+/-	²²⁶ Ra (pCi/g)	+/-	²³⁸ U (pCi/g)	+/-	²³² Th (pCi/g)	+/-	¹³⁷ Cs (pCi/g)	+/-
148-152	0.327	79.9	0.42	0.10	0.11	0.10	0.318	0.010	1.562	0.093	0.344	0.017	n.d.	n.d.
152-156	0.326	90.1	0.26	0.10	0.00	0.10	0.338	0.010	1.150	0.074	0.423	0.019	n.d.	n.d.
156-160	0.321	89.7	0.42	0.08	0.11	0.08	0.308	0.008	0.841	0.070	0.421	0.016	n.d.	n.d.
160-164	0.327	51.3	0.42	0.08	0.15	0.08	0.252	0.008	3.926	0.102	0.339	0.015	n.d.	n.d.
164-168	0.491	37.2	0.26	0.09	0.00	0.10	0.353	0.009	5.743	0.123	0.334	0.013	n.d.	n.d.
168-172	0.517	38.3	0.56	0.07	0.23	0.07	0.331	0.008	4.631	0.090	0.250	0.009	n.d.	n.d.
172-176	0.385	37.4	0.30	0.09	0.00	0.10	0.395	0.011	5.067	0.127	0.357	0.014	n.d.	n.d.
176-180	0.494	36.9	0.33	0.08	0.00	0.10	0.345	0.009	4.813	0.098	0.293	0.010	n.d.	n.d.
180-184	0.417	36.8	0.25	0.09	0.00	0.10	0.324	0.010	5.259	0.121	0.269	0.010	n.d.	n.d.
184-188	0.607	29.8	0.50	0.09	0.20	0.09	0.295	0.009	8.645	0.143	0.225	0.009	0.012	0.006
188-192	0.397	41.9	0.58	0.08	0.24	0.08	0.343	0.009	6.085	0.106	0.277	0.009	n.d.	n.d.
192-196	0.414	46.1	0.31	0.09	0.00	0.10	0.353	0.010	5.921	0.123	0.338	0.014	n.d.	n.d.
196-200	0.565	45.7	0.31	0.09	0.03	0.09	0.352	0.010	5.283	0.122	0.298	0.013	n.d.	n.d.

Errors based on counting statistics ($\pm 1\sigma$); n.d., not detected.

^aDetrital Fraction (%) = $[1 - (\text{CaCO}_3 + \text{C}_{\text{org}} + \text{S})] \cdot 100$. Concentrations of CaCO₃, C_{org}, and S from Glenn et al. (1995).

ties are more fully discussed in Glenn et al. (1995). ²²⁶Ra activities are generally constant with depth. Cores G-8 and M-21 both display ²²⁶Ra activity peaks within the topmost 20 cm that decrease near the core top (Figure 4). As expected from its geochemical behavior, ²³²Th activities appear to reflect detrital material, being somewhat inversely correlated with calcium carbonate, as reflected in the ²³⁸U activities in Figure 4. ²³²Th activities appear to covary with those of ²²⁶Ra, especially in the topmost portion of cores G-8 and M-21, suggesting a detrital origin for both radionuclides.

²¹⁰Pb Modeling

The disequilibrium between ²¹⁰Pb and ²²⁶Ra was first utilized to date recent (<150 yr) lake and nearshore marine sediments by Krishnaswami et al. (1971) and Koide et al. (1972, 1973). Krishnaswami et al. (1971) presented a simple model that successfully explained their ²¹⁰Pb profiles based upon a constant flux of excess ²¹⁰Pb to the sediment-water interface and a constant sedimentation rate. Additional assumptions in their model are as follows: (1) no postdepositional migration of the nuclide within the sediment (i.e., no nuclide diffusion or physical mixing of the sediment by bioturbation, considered a reasonable assumption for the anoxic sediments studied here); and (2) the activity of ²¹⁰Pb supported by ²²⁶Ra in the sediment is independent of depth (not considered here because we have measured the ²²⁶Ra activity for each sample interval). Under the conditions of this simple, steady-state model, the activity (*A*) of a sediment section of age *t* is

$$A(t) = (F/\omega)e^{-\lambda t} + A' \quad (1)$$

where *F* is the flux of ²¹⁰Pb at the sediment-water interface in pCi cm⁻² yr⁻¹, ω is the bulk sediment accumulation rate in g cm⁻² yr⁻¹ (combining the section depth interval in cm with the sediment dry bulk density in g cm⁻³), *A'* is the activity of ²¹⁰Pb supported by ²²⁶Ra in pCi g⁻¹ dry weight, and λ is the radioactive decay constant for ²¹⁰Pb ($= \ln 2/t_{1/2}$ where $t_{1/2} = 22.3$ yr, or 0.031 yr⁻¹).

Robbins (1978) introduced two useful

TABLE 5

CENTRAL HONOLULU WATERSHED SOILS AND STREAMS: URANIUM- AND THORIUM-SERIES RADIONUCLIDE AND FALLOUT ^{137}Cs ACTIVITIES

SAMPLE IDENTITY	^{210}Pb (pCi/g)		Ex. ^{210}Pb (pCi/g)		^{226}Ra (pCi/g)		Ex. ^{226}Ra (pCi/g)		^{238}U (pCi/g)		^{232}Th (pCi/g)		^{137}Cs (pCi/g)	
		+/-		+/-		+/-		+/-		+/-		+/-		+/-
Soil 92-5														
0-10 cm	0.751	0.104	-0.415	0.105	1.17	0.015	0.088	0.072	1.15	0.071	1.41	0.024	0.178	0.010
10-20 cm	0.501	0.075	-0.655	0.076	1.16	0.011	0.121	0.061	1.04	0.060	1.32	0.015	0.316	0.009
20-30 cm	0.395	0.097	-0.836	0.098	1.23	0.016	0.070	0.081	1.16	0.079	1.30	0.019	0.164	0.010
30-40 cm	0.887	0.084	-0.226	0.085	1.11	0.012	0.242	0.064	0.871	0.063	1.10	0.015	0.070	0.006
40-50 cm	0.738	0.076	-0.387	0.077	1.12	0.011	0.144	0.061	0.981	0.060	1.08	0.013	0.050	0.005
Soil 92-6														
0-10 cm	0.681	0.091	-0.034	0.092	0.715	0.012	0.029	0.069	0.686	0.068	0.855	0.017	0.170	0.009
10-20 cm	0.611	0.094	-0.095	0.094	0.706	0.012	0.227	0.070	0.479	0.069	0.787	0.016	0.136	0.009
20-30 cm	0.223	0.079	-0.475	0.080	0.698	0.010	0.250	0.060	0.448	0.059	0.725	0.013	0.081	0.006
30-40 cm	0.231	0.092	-0.497	0.093	0.728	0.013	0.154	0.061	0.595	0.059	0.704	0.017	0.036	0.007
40-50 cm	0.284	0.081	-0.353	0.081	0.637	0.010	-0.072	0.064	0.709	0.064	0.677	0.014	0.005	0.005
Soil 92-7														
0-10 cm	6.96	0.137	6.04	0.138	0.911	0.012	-0.162	0.072	1.07	0.071	1.87	0.017	2.67	0.030
10-20 cm	3.54	0.141	2.05	0.142	1.49	0.017	-0.323	0.094	1.81	0.093	2.22	0.022	2.19	0.032
20-30 cm	0.582	0.102	-1.11	0.104	1.69	0.017	0.452	0.081	1.24	0.079	1.84	0.023	0.173	0.010
30-40 cm	0.406	0.105	-1.45	0.107	1.85	0.019	0.574	0.089	1.28	0.087	1.93	0.026	0.037	0.007
40-50 cm	0.650	0.114	-1.21	0.116	1.86	0.019	0.586	0.069	1.30	0.066	2.08	0.027	0.049	0.007
Soil 92-9														
0-10 cm	1.54	0.103	1.10	0.103	0.443	0.010	-0.123	0.070	0.566	0.069	0.788	0.013	0.951	0.021
10-20 cm	0.126	0.079	-0.509	0.080	0.635	0.010	-0.109	0.066	0.744	0.065	0.741	0.013	0.256	0.010
20-30 cm	n.d.	n.d.	-0.591	0.012	0.591	0.012	-0.076	0.079	0.667	0.078	0.651	0.016	0.199	0.011
30-40 cm	0.352	0.081	-0.267	0.082	0.619	0.010	0.166	0.067	0.453	0.066	0.661	0.015	0.048	0.006
40-50 cm	n.d.	n.d.	-0.423	0.009	0.423	0.009	0.105	0.072	0.318	0.072	0.453	0.016	0.035	0.007
Soil 92-10														
0-10 cm	0.909	0.112	0.089	0.113	0.819	0.015	0.093	0.084	0.727	0.083	0.827	0.017	0.289	0.013
10-20 cm	0.595	0.107	-0.765	0.109	1.36	0.018	0.151	0.097	1.21	0.095	1.36	0.023	0.082	0.009
20-30 cm	0.244	0.085	-1.21	0.086	1.45	0.015	0.505	0.072	0.948	0.070	1.38	0.018	0.021	0.005
30-40 cm	0.672	0.104	-0.750	0.105	1.42	0.017	0.131	0.064	1.27	0.062	1.37	0.020	0.005	0.005
40-50 cm	0.471	0.085	-0.218	0.086	0.689	0.009	0.135	0.060	0.554	0.059	0.760	0.013	0.024	0.004
Soil 92-13														
0-10 cm	1.19	0.086	0.407	0.087	0.783	0.012	0.026	0.068	0.757	0.067	0.987	0.015	0.734	0.017
10-20 cm	0.837	0.088	-0.048	0.089	0.885	0.012	0.276	0.068	0.609	0.066	1.02	0.016	0.424	0.013
20-30 cm	0.257	0.087	-0.748	0.088	1.00	0.013	0.280	0.071	0.726	0.070	1.04	0.017	0.242	0.011
30-40 cm	0.044	0.085	-0.725	0.086	0.769	0.013	-0.038	0.077	0.807	0.076	0.760	0.017	0.023	0.006
40-50 cm	0.488	0.092	-0.539	0.093	1.03	0.014	-0.169	0.083	1.20	0.081	1.06	0.019	0.036	0.007
50-60 cm	0.385	0.091	-0.857	0.092	1.24	0.016	0.281	0.080	0.962	0.078	1.38	0.023	0.126	0.009

60-70 cm	0.046	0.085	-0.810	0.086	0.856	0.014	0.238	0.076	0.618	0.075	0.870	0.019	0.036	0.007
70-80 cm	0.105	0.085	-0.306	0.085	0.411	0.010	-0.074	0.054	0.485	0.053	0.470	0.015	0.051	0.007
80-90 cm	0.163	0.087	-0.272	0.088	0.435	0.010	-0.077	0.073	0.512	0.073	0.484	0.016	0.059	0.008
90-100 cm	0.060	0.070	-0.357	0.071	0.417	0.008	-0.094	0.060	0.511	0.059	0.445	0.011	0.049	0.006
Soil 92-14														
0-10 cm	4.78	0.114	4.01	0.115	0.773	0.012	0.017	0.067	0.756	0.066	1.51	0.014	2.30	0.028
10-20 cm	1.06	0.088	-0.252	0.089	1.32	0.013	0.534	0.063	0.782	0.062	1.42	0.016	0.281	0.010
20-30 cm	0.526	0.093	-0.753	0.094	1.28	0.015	0.831	0.070	0.448	0.068	1.30	0.019	n.d.	n.d.
30-40 cm	0.813	0.093	-0.636	0.094	1.45	0.014	0.297	0.073	1.15	0.072	1.50	0.018	0.019	0.005
40-50 cm	0.712	0.093	-0.553	0.094	1.27	0.014	0.039	0.077	1.23	0.076	1.40	0.021	0.011	0.004
Soil 93-15														
0-50 cm ^a	1.63	0.086	1.55	0.086	0.081	0.005	-0.056	0.056	0.137	0.056	0.268	0.008	0.617	0.014
0-10 cm	4.21	0.134	4.14	0.134	0.074	0.006	-0.175	0.069	0.249	0.069	0.369	0.008	0.902	0.021
10-20 cm	1.99	0.093	1.84	0.093	0.151	0.005	0.049	0.059	0.102	0.059	0.545	0.009	1.11	0.019
20-30 cm	0.736	0.096	0.675	0.096	0.061	0.005	-0.242	0.067	0.303	0.067	0.364	0.010	0.753	0.018
30-40 cm	0.443	0.095	0.359	0.095	0.085	0.006	-0.093	0.068	0.178	0.067	0.196	0.009	0.355	0.014
40-50 cm	0.587	0.080	0.485	0.080	0.102	0.005	-0.019	0.056	0.121	0.055	0.141	0.007	0.223	0.009
Soil 93-16														
0-50 cm ^a	0.868	0.096	0.740	0.096	0.128	0.006	-0.139	0.069	0.267	0.068	0.283	0.013	0.324	0.013
0-10 cm	2.47	0.120	2.38	0.121	0.086	0.005	0.086	0.005	n.d.	n.d.	0.452	0.008	1.19	0.023
10-20 cm	0.983	0.095	0.890	0.095	0.093	0.004	-0.060	0.059	0.153	0.059	0.280	0.009	0.469	0.013
20-30 cm	n.d.	n.d.	-0.130	0.004	0.130	0.004	0.034	0.055	0.096	0.055	0.121	0.007	0.095	0.006
30-40 cm	n.d.	n.d.	-0.173	0.007	0.173	0.007	-0.188	0.070	0.361	0.069	0.202	0.013	0.042	0.007
40-50 cm	n.d.	n.d.	-0.142	0.006	0.142	0.006	-0.242	0.066	0.384	0.066	0.184	0.011	0.011	0.005
Soil 93-17														
0-50 cm ^a	1.04	0.100	0.524	0.100	0.516	0.011	0.089	0.072	0.427	0.072	0.729	0.017	0.591	0.017
0-10 cm	3.24	0.125	2.664	0.126	0.582	0.010	-0.252	0.072	0.834	0.071	1.15	0.013	1.76	0.026
10-20 cm	1.22	0.097	0.657	0.097	0.563	0.009	-0.325	0.067	0.888	0.066	0.906	0.014	0.790	0.016
20-30 cm	0.679	0.078	0.076	0.079	0.603	0.008	0.117	0.056	0.486	0.056	0.750	0.011	0.380	0.010
30-40 cm	0.303	0.091	-0.211	0.092	0.514	0.010	0.211	0.068	0.303	0.068	0.502	0.013	0.035	0.006
40-50 cm	0.078	0.083	-0.301	0.083	0.379	0.009	0.009	0.064	0.370	0.064	0.411	0.012	0.007	0.005
Soil 93-18														
0-50 cm ^a	1.16	0.088	0.613	0.088	0.543	0.009	0.228	0.061	0.314	0.061	0.764	0.014	0.690	0.015
0-10 cm	3.45	0.106	2.496	0.107	0.956	0.011	0.005	0.064	0.950	0.063	1.57	0.015	1.85	0.023
10-20 cm	1.85	0.106	0.903	0.107	0.946	0.013	0.001	0.074	0.945	0.073	1.38	0.016	1.38	0.023
20-30 cm	0.445	0.094	-0.470	0.095	0.915	0.013	0.086	0.076	0.829	0.074	1.12	0.018	0.617	0.017
30-40 cm	0.028	0.082	-0.614	0.083	0.642	0.011	-0.005	0.072	0.647	0.071	0.639	0.013	0.057	0.007
40-50 cm	n.d.	n.d.	-0.463	0.011	0.463	0.011	0.127	0.078	0.336	0.077	0.496	0.018	n.d.	n.d.
Soil 93-19														
0-50 cm ^a	1.25	0.083	1.10	0.084	0.157	0.006	-0.260	0.060	0.417	0.059	0.464	0.009	0.870	0.017
0-10 cm	5.24	0.132	5.05	0.132	0.188	0.007	-0.134	0.063	0.322	0.063	1.01	0.010	2.49	0.031
10-20 cm	0.813	0.082	0.640	0.082	0.172	0.006	0.025	0.059	0.148	0.059	0.587	0.009	1.27	0.020
20-30 cm	0.246	0.090	0.015	0.090	0.230	0.007	-0.005	0.065	0.235	0.065	0.285	0.011	0.259	0.012

TABLE 5 (continued)

SAMPLE IDENTITY	^{210}Pb		Ex. ^{210}Pb		^{226}Ra		Ex. ^{226}Ra		^{238}U		^{232}Th		^{137}Cs	
	(pCi/g)	+/-	(pCi/g)	+/-	(pCi/g)	+/-	(pCi/g)	+/-	(pCi/g)	+/-	(pCi/g)	+/-	(pCi/g)	+/-
30-40 cm	0.055	0.084	-0.088	0.084	0.143	0.006	0.075	0.051	0.068	0.050	0.235	0.014	0.023	0.006
40-50 cm	0.163	0.074	0.001	0.075	0.162	0.006	0.109	0.057	0.053	0.056	0.170	0.009	0.065	0.006
Soil 93-20														
0-50 cm ^a	0.192	0.086	-0.065	0.087	0.257	0.008	0.131	0.069	0.126	0.068	0.358	0.011	0.421	0.015
0-10 cm	1.02	0.087	0.827	0.087	0.197	0.006	-0.091	0.059	0.288	0.059	0.506	0.011	0.851	0.018
10-20 cm	0.433	0.085	0.201	0.085	0.232	0.007	0.093	0.063	0.139	0.063	0.398	0.011	0.527	0.016
20-30 cm	0.246	0.067	0.070	0.067	0.176	0.005	0.123	0.050	0.053	0.049	0.263	0.008	0.311	0.010
30-40 cm	0.236	0.079	0.051	0.080	0.185	0.006	-0.010	0.059	0.195	0.059	0.290	0.011	0.243	0.010
40-50 cm	0.146	0.084	0.008	0.084	0.138	0.006	0.104	0.032	0.017	0.031	0.197	0.010	0.129	0.009
Soil 93-21														
0-50 cm ^a	0.465	0.085	0.140	0.086	0.325	0.008	0.120	0.063	0.205	0.062	0.450	0.013	0.446	0.014
0-10 cm	1.50	0.081	1.29	0.082	0.209	0.006	-0.067	0.053	0.276	0.052	0.502	0.008	0.896	0.016
10-20 cm	0.755	0.088	0.531	0.089	0.223	0.007	0.098	0.060	0.125	0.060	0.447	0.012	0.672	0.017
20-30 cm	0.562	0.072	0.313	0.072	0.249	0.006	0.200	0.050	0.049	0.050	0.352	0.008	0.359	0.010
30-40 cm	0.263	0.086	-0.136	0.087	0.399	0.010	0.098	0.067	0.301	0.067	0.368	0.011	0.151	0.009
40-50 cm	0.136	0.079	-0.221	0.080	0.357	0.008	0.357	0.036	0.214	0.035	0.400	0.011	0.057	0.006
Stream 92-1														
45-1,000 μm	0.948	0.082	0.840	0.082	0.111	0.005	-0.029	0.053	0.140	0.052	0.215	0.007	0.342	0.011
<45 μm	3.42	0.134	3.18	0.134	0.247	0.009	0.115	0.009	n.d.	n.d.	0.584	0.014	0.888	0.023
Stream 92-2														
45-1,000 μm	0.293	0.061	0.021	0.062	0.272	0.005	0.174	0.041	0.098	0.041	0.309	0.007	0.120	0.005
<45 μm	5.92	0.146	5.17	0.147	0.751	0.013	0.266	0.072	0.486	0.071	1.09	0.018	1.07	0.023
Stream 92-3														
45-1,000 μm	1.94	0.118	1.34	0.119	0.601	0.013	0.375	0.081	0.226	0.080	0.792	0.020	0.478	0.018
<45 μm	4.03	0.106	3.58	0.106	0.442	0.008	0.159	0.054	0.283	0.053	0.588	0.010	0.539	0.013
Stream 92-4														
45-1,000 μm	1.31	0.131	1.00	0.131	0.309	0.013	-0.302	0.418	0.611	0.418	0.355	0.017	0.239	0.016
<45 μm	6.52	0.205	6.15	0.205	0.370	0.013	-1.37	0.126	1.74	0.125	0.598	0.017	0.898	0.027
Stream 92-8														
45-1,000 μm	0.571	0.079	0.210	0.08	0.361	0.008	0.001	0.059	0.360	0.058	0.374	0.010	0.212	0.009
<45 μm	1.66	0.113	1.17	0.114	0.483	0.011	0.129	0.074	0.354	0.073	0.606	0.015	0.419	0.016
Stream 92-11														
45-1,000 μm	0.295	0.080	-0.021	0.080	0.316	0.007	-0.149	0.055	0.465	0.055	0.392	0.009	0.172	0.007
<45 μm	1.72	0.097	1.15	0.098	0.573	0.010	-0.113	0.071	0.686	0.070	0.744	0.016	0.395	0.013
Stream 92-12														
45-1,000 μm	0.835	0.085	0.320	0.086	0.514	0.009	0.213	0.043	0.285	0.042	0.607	0.012	0.218	0.009
<45 μm	3.43	0.126	2.44	0.126	0.993	0.015	0.082	0.079	0.911	0.078	1.13	0.018	0.597	0.018

Errors based on counting statistics ($\pm 1\sigma$); n.d., not detected.^a Composite sample.

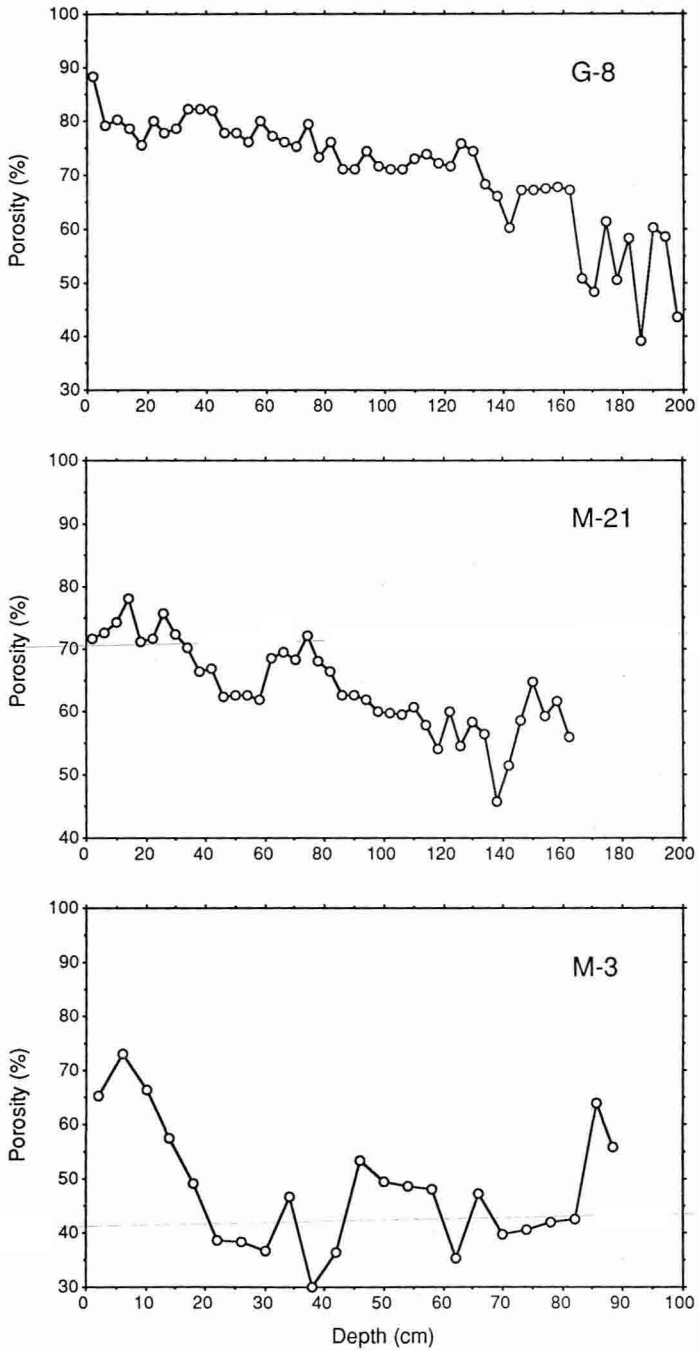


FIGURE 3. Distribution of porosity with depth for Ala Wai sediment cores. Points are medians of 4-cm-wide sampling intervals.

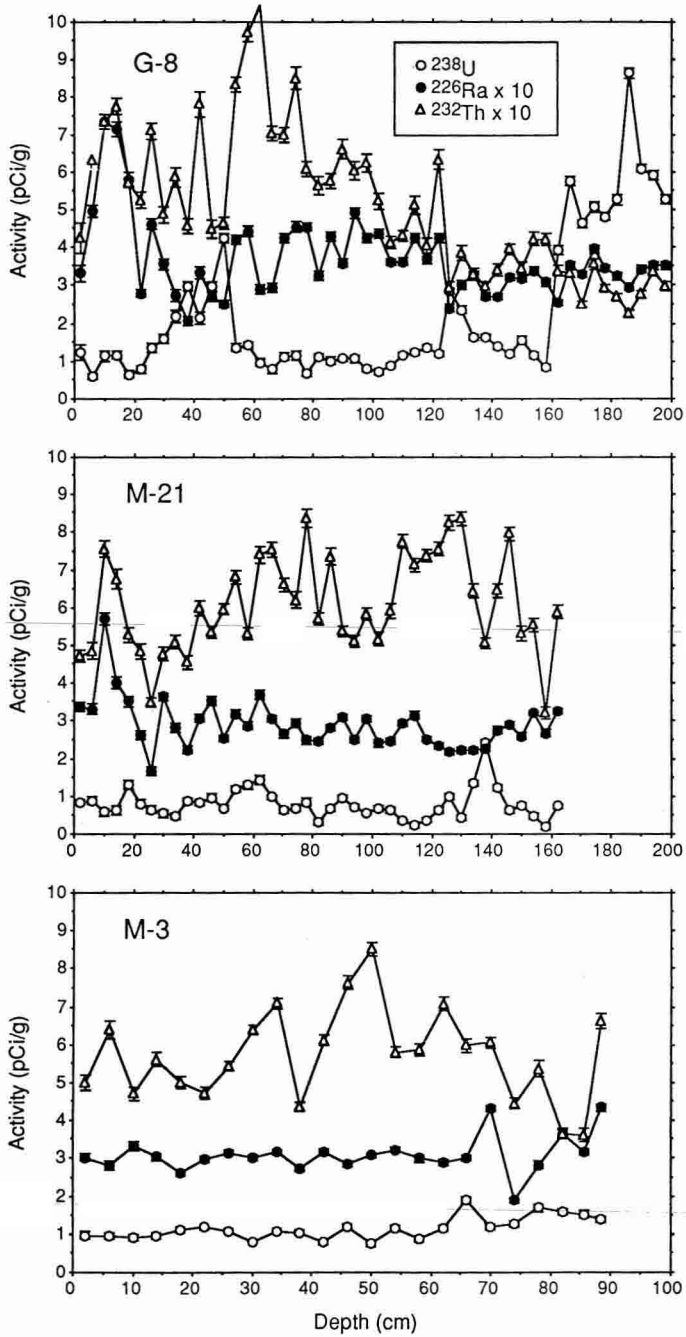


FIGURE 4. Distribution of ^{238}U , ^{226}Ra , and ^{232}Th activities with depth for Ala Wai Canal sediment cores.

variations on the simple, steady-state model for the distribution of ^{210}Pb in sediments and the determination of sedimentation rates: the constant flux and constant activity models. In the constant flux model, the sedimentation rate is variable, but the delivery of excess ^{210}Pb remains constant; there is variable dilution of the excess ^{210}Pb flux by the bulk sediments (Robbins 1978). The time-invariant flux for the constant flux model is

$$F = \lambda I^* \quad (2)$$

where I^* is the total integrated excess ^{210}Pb inventory in the sediment column (pCi cm^{-2}). The age T (yr B.P.) of a sediment horizon at a mass-depth m (units of g cm^{-2}) is given by

$$T(m) = \lambda^{-1} \ln[1 - \lambda I(m)/F]^{-1} \quad (3)$$

where $I(m)$ is the excess ^{210}Pb inventory between m and the sediment surface (Smith et al. 1987). This model has been successful in characterizing the sedimentation in many fluvial-marine systems (Robbins and Edgington 1975, Robbins 1978, Smith and Ellis 1982, Smith et al. 1987, Edgington et al. 1991).

The constant activity model considers the case of nonconstant ^{210}Pb fluxes, where there is variable sedimentation of material having constant specific activity. In terms of the "depth"-age relationship, the constant activity model is equivalent to the simple model, so that age T (yr B.P.) of a sediment horizon at a mass-depth m (units of g cm^{-2}) is given by

$$T(m) = \lambda^{-1} \ln[(A - A')/(A - A')_0]^{-1} \quad (4)$$

where $(A - A')_0$ is the initial or surface excess ^{210}Pb activity (Robbins 1978).

Figure 5 displays the depth distributions of excess ^{210}Pb activity for the three Ala Wai Canal cores studied. Depths in centimeters are shown solely because they are more intuitive. Strictly, "depths" in mass-depth units of g cm^{-2} are more accurate because of the effects of sediment compaction and variable downcore porosity on the nuclide-specific activities (Figure 3) (Robbins and Edgington 1975, Robbins 1978). These units were used in the age calculations. In spite of corrections for dilution by the various marine authigenic

phases (Figure 5) and conversion of linear depth to mass-depth units (not shown), the Ala Wai sediments cannot be described by a simple model involving a constant sedimentation rate. Multiple episodes of sedimentation rate changes are evident by slope changes in all cores, which were fitted by model 1 linear regression analysis. Model 2 regression analysis is preferred for these fits (Snidvongs et al. 1995), but no significant differences between these two statistical models were noted for those fits with $r > 0.9$, and the errors of the remaining regression fits in Figure 5 are so large that additional statistical interpretation is unwarranted. The extrapolated surface excess ^{210}Pb activity ranges from about 3 to 5 pCi g^{-1} (Figure 5). These values are comparable with surface excess ^{210}Pb activities from about 3 to 4 pCi g^{-1} for carbonate-rich sediments within Kāne'ohe Bay, O'ahu (C. R. Smith and G.M.M., unpublished data). However, because the Kāne'ohe Bay sediments are known to contain a near-surface mixing zone caused by bioturbation, the Ala Wai Canal surface excess ^{210}Pb activities may actually be too low, suggesting either some core-top loss during recovery or erosion of the near-surface sediment before coring.

Sediment age-versus-depth profiles based on the excess ^{210}Pb constant flux and constant activity models are presented in Figure 6. Because the age of the canal is known and there is little possibility that the cores penetrated into older, pre-canal material (likely to be indurated limestone [Glenn and McMurtry 1995]), a useful upper limit of about 64 yr can be assigned to the sediments (Figure 6). It is evident from Figure 6 that there is little agreement between the models and that both models predict ages older than that possible for the canal. In the upper portion of the canal sediment, the constant flux model generally gives sedimentation rates that are equal to or faster than those generated by the constant activity model (core M-21 being the exception). These trends reverse in the lower portions of the sediment column, with the constant flux model indicating slower rates, but the uncertainties of the derived ages in both models are comparatively large in these

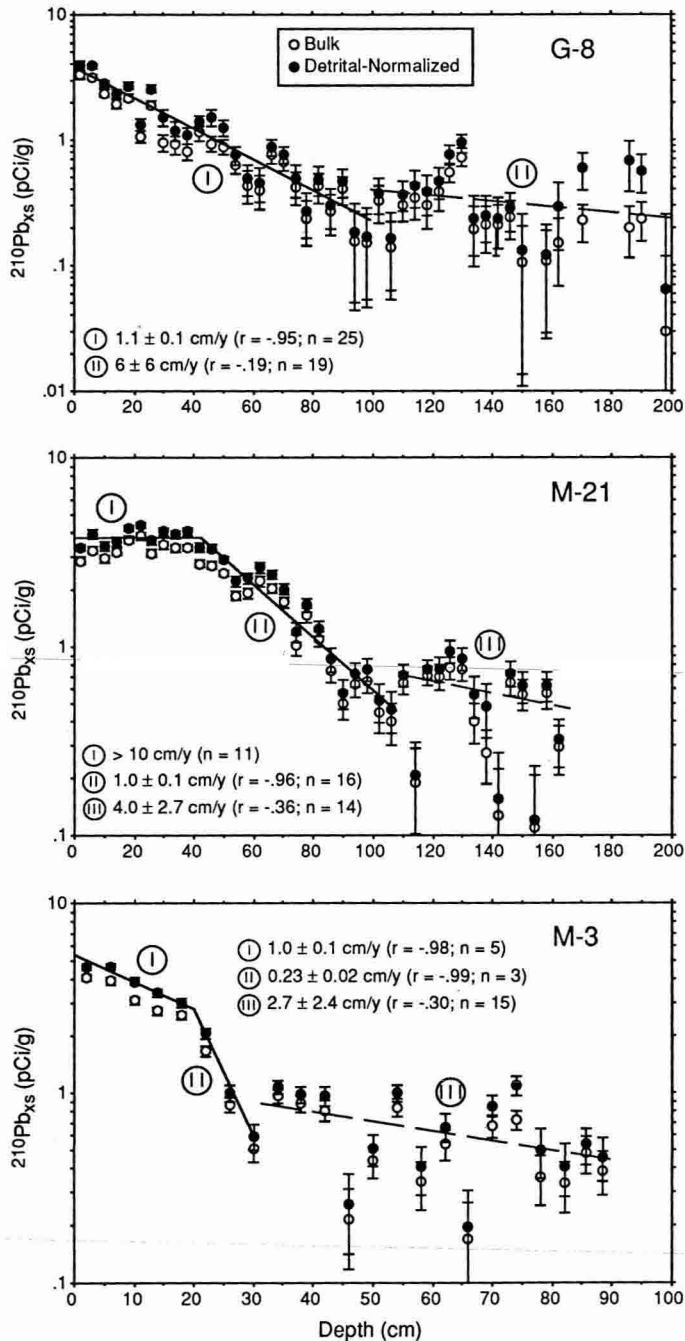


FIGURE 5. Distribution of excess ^{210}Pb activity with depth for Ala Wai Canal sediment cores. Detrital-normalized activities were calculated to remove dilution effects of authigenic carbonates, organic matter, and sulfur of marine origin, assuming that most of the ^{210}Pb activity resides in detrital clays transported from the watershed. Sedimentation rates are derived from model 1 regression fits.

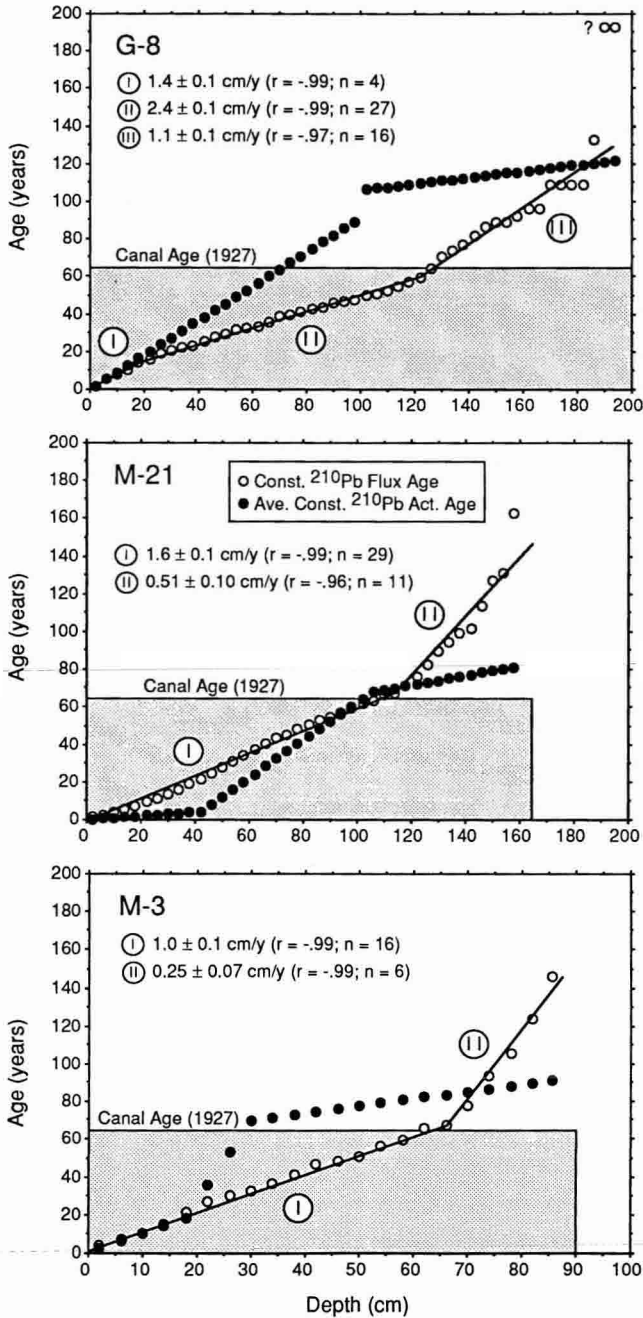


FIGURE 6. Excess ^{210}Pb interval age versus depth for Ala Wai Canal sediment cores. Ages based on two ^{210}Pb models, constant flux and constant specific activity (Robbins 1978), are compared with the actual "space-time" of each canal core (shaded box). For the constant specific activity model, average ages are shown based on the regression fits in Figure 3. Constant flux model sedimentation rates are derived from model 1 regression fits. Uncertainties are minimum values based solely on the standard error of the regression.

areas because of the large statistical errors for excess ^{210}Pb as the level of ^{226}Ra support is approached (Figures 5 and 6).

The range of excess ^{210}Pb sedimentation rates for the Ala Wai Canal sediments (from 0.2 to > 10 cm/yr, with most values from 1 to 4 cm/yr) is consistent with values typical of estuarine and coastal embayment sedimentation elsewhere (Hirschberg and Schubel 1979, Smith and Ellis 1982, Smith et al. 1987, Sugai 1990, Sugai et al. 1994, Snidvongs et al. 1995). Furthermore, significant differences in sedimentation rates among various steady-state models of excess ^{210}Pb geochronology are not uncommon (e.g., Robbins 1978). This widely used and often reliable dating method would, however, yield misleading results for the Ala Wai Canal sediments if the age of this estuary were unknown or if no other, independent dating method was utilized.

^{137}Cs Modeling

Fallout ^{137}Cs , a nuclear fission product with $t_{1/2} = 30.1$ yr, was first introduced to the environment with the advent of nuclear weapons testing in 1945. Considerable global distribution of this nuclide was produced by high-yield, aboveground thermonuclear tests that began in 1952 and largely culminated in a 2-yr period between 1961 and 1962 when, before the cessation of aboveground testing with the nuclear test-ban treaty in 1963, about 60% of all atmospheric detonation yields between 1945 and 1975 occurred (Carter and Moghissi 1977). After introduction into the stratosphere, ^{137}Cs moves with other fallout debris back into the troposphere, where deposition at the earth's surface is strongly related to local precipitation (Ritchie and McHenry 1990). After deposition, ^{137}Cs is almost irreversibly adsorbed onto the cation exchange sites of soils (clay minerals and clay-sized amorphous material), with low permanent uptake onto organic matter. Fallout ^{137}Cs moves through watersheds primarily by soil erosion and transport; final deposition is usually from suspended material into water bodies (Ritchie and McHenry 1990 and references therein).

The depth distribution of ^{137}Cs activity

for the three Ala Wai Canal cores is presented in Figure 7. In an ideal aquatic environment with direct fallout as the sole source of ^{137}Cs and no postdepositional migration, the sedimentation rate can be estimated from the reflection of the known atmospheric deposition record (e.g., HASL 1977) in the ^{137}Cs depth distribution. Most aquatic environments, however, contain intermediate reservoirs between the atmosphere and the sediment, such as watershed soils and lakes, that complicate the ^{137}Cs depositional record by gradual release to the sedimentary pool (Smith and Ellis 1982, Smith et al. 1987; Snidvongs et al. 1995). Average, overall sedimentation rates can still be estimated from the level of first detection (corresponding to ca. 1952), provided that there is no postdepositional migration from physical mixing or diffusion of ^{137}Cs and assuming a relatively short water-column residence time of 1 yr (Smith et al. 1987) or less.

Because the clay-rich lithology of the anoxic Ala Wai sediments is comparable with those of sediments from other coastal areas where ^{137}Cs is shown to be immobile (Sugai et al. 1994, Snidvongs et al. 1995), postdepositional migration of ^{137}Cs is likely to be negligible. Nevertheless, desorption and diffusion of ^{137}Cs might affect the sedimentation rate estimation. These mechanisms can cause ^{137}Cs to penetrate deeper into the sediment than the actual solid accumulation thickness. This possibility can be assessed by a simple one-dimensional diffusion model where the diffusive flux of desorped ^{137}Cs (J_{Cs}) can be calculated from the activity gradient in the pore solution using:

$$J_{\text{Cs}} = -\phi \cdot D_{\text{Cs,pw}} \cdot \frac{dC_{\text{Cs,pw}}}{dz} \quad (5)$$

where ϕ is porosity, $D_{\text{Cs,pw}}$ is the effective diffusion coefficient of ^{137}Cs in porewater, and $dC_{\text{Cs,pw}}/dz$ is the vertical concentration (or activity) gradient of dissolved ^{137}Cs in porewater (Berner 1980).

Because the effective diffusion coefficients in porewater are related to the diffusion coefficients in free solution (Berner 1980), and the activity of the desorped fraction is also

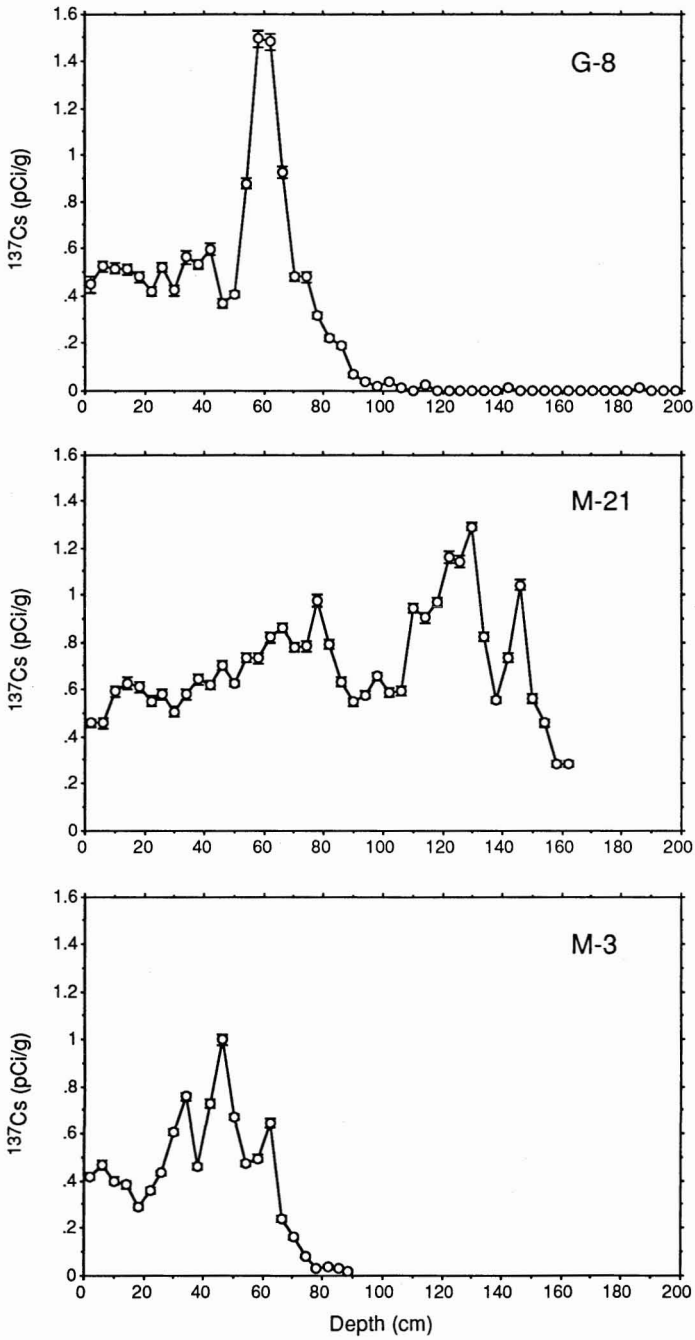


FIGURE 7. Distribution of ^{137}Cs activity with sampling depth for Ala Wai Canal sediment cores.

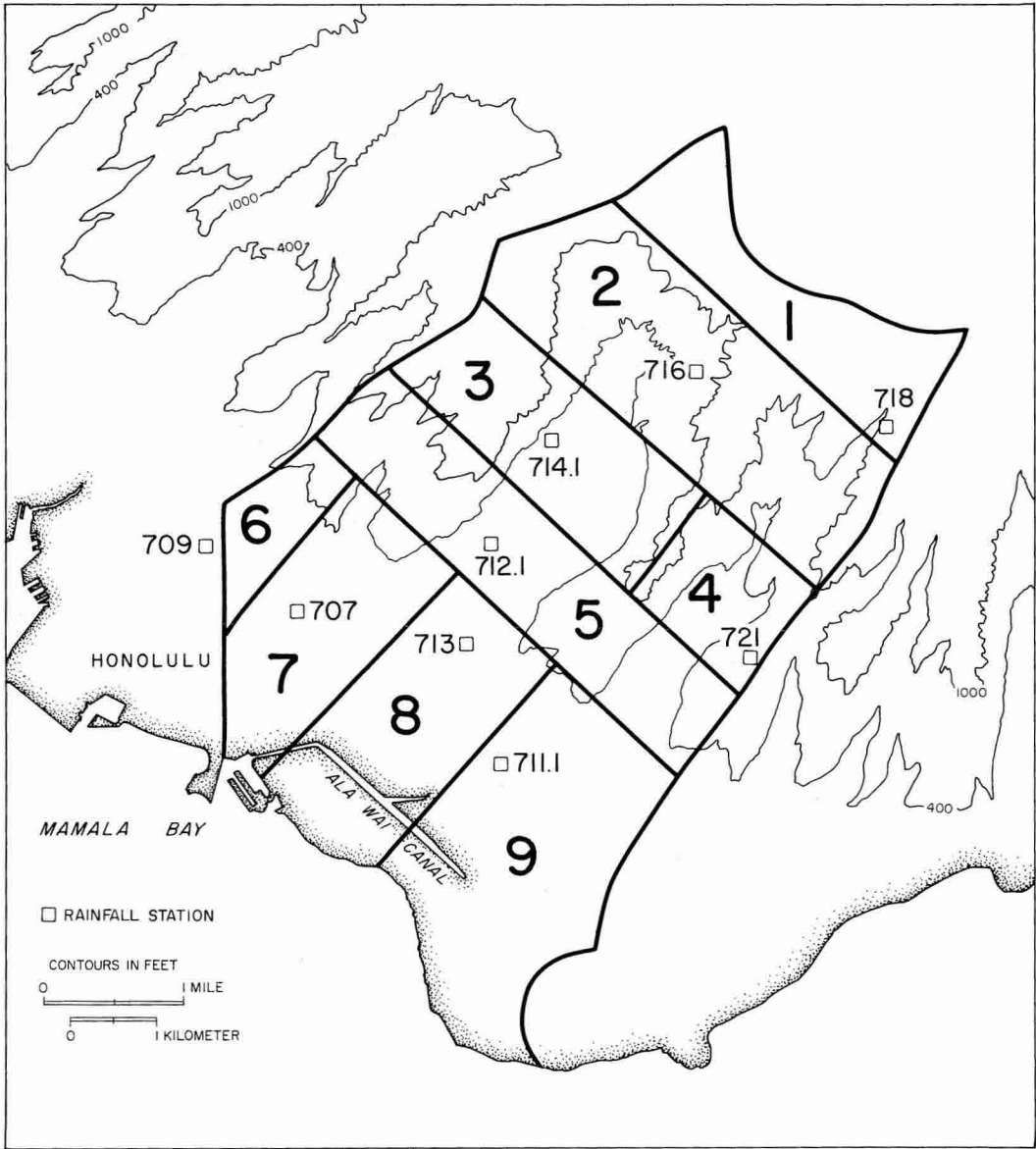


FIGURE 8. Topographic contour map of the central Honolulu watershed, showing the nine segments and corresponding rainfall stations used in the fallout ¹³⁷Cs mass-balance model.

related to the total activity, equation 5 can be written as:

$$J_{Cs} = -\frac{\phi}{\theta^2} \cdot \frac{1}{1 + K_{Cs}} \cdot D_{Cs,o} \cdot \frac{dA_{Cs}}{dz} \quad (6)$$

where θ is the tortuosity, $D_{Cs,o}$ is the diffusion coefficient of Cs in seawater, K_{Cs} is the distribution coefficient for Cs, and dA_{Cs}/dz is the observed vertical gradient of ¹³⁷Cs in the sediment.

TABLE 6
CENTRAL HONOLULU WATERSHED AND ALA WAI CANAL ¹³⁷Cs INVENTORIES

CENTRAL HONOLULU WATERSHED				ALA WAI CANAL					
SEGMENT NO.	RAIN GAUGE NO.	AREA (km ²)	PREDICTED ¹³⁷ Cs SOIL ACTIVITY (pCi/cm ²)	TOTAL PREDICTED ¹³⁷ Cs ACTIVITY (mCi)	SEGMENT	CORE NO.	AREA (m ²)	¹³⁷ Cs SPECIFIC ACTIVITY (pCi/cm ²)	TOTAL ¹³⁷ Cs ACTIVITY (mCi)
1	718	4.6	27.32	1,257	Inner	G-8	36,250	11.21	4.07
2	716	8.0	30.82	2,466	Middle	M-21	112,500	42.31	47.60
3	714.1	4.8	21.31	1,023	Outer	M-3	40,000	19.42	7.77
4	720	2.6	9.04	235	Total	—	188,750	—	59.43
5	712.1	6.5	9.26	602					
6	709	1.4	7.38	103					
7	707	4.5	7.07	318					
8	713	4.5	7.44	335					
9	711.1	6.0	5.54	332					
Total	—	42.9	—	6,671					

The values for ϕ/θ^2 for most surface marine sediments are usually not more than 0.5 (Berner 1980). The Cs diffusion coefficient in free solution is about $2 \times 10^{-5} \text{ cm}^2 \text{ sec}^{-1}$ (Li and Gregory 1974). The lowest known K_{Cs} in natural sediments is about $100 \text{ cm}^3 \text{ g}^{-1}$ (Gillham et al. 1980, Santschi et al. 1983, Nyffeler et al. 1984, Torgersen and Longmore 1984). The steepest gradient dA_{Cs}/dz found in profiles during this study is about $-0.03 \text{ pCi g}^{-1} \text{ cm}^{-1}$ for core M-21 (Figure 7). By using these values, the maximum diffusive flux would be about $0.09 \text{ pCi cm}^{-2} \text{ yr}^{-1}$ downward. This calculated maximum diffusive flux is only about 10% of the total influx of ¹³⁷Cs to the sediment-water interface (I_{Cs}) of $0.97 \text{ pCi cm}^{-2} \text{ yr}^{-1}$ for core M-21. Because the most likely diffusive flux may be appreciably less than this $0.09 \text{ pCi cm}^{-2} \text{ yr}^{-1}$, it can be concluded that the desorption and diffusion of ¹³⁷Cs cannot cause major discrepancies in the sedimentation rate estimation.

We thus obtained average, overall sedimentation rates for cores G-8, M-21, and M-3 of 2.5, >4.2, and 2.3 cm/yr, respectively; however, we wished to obtain more detailed information on the sedimentation history as well as on the erosional flux from the watershed to the canal. To accomplish these goals, we applied a ¹³⁷Cs erosion/redeposition model that utilizes a nonsteady-state, two-box model of the ¹³⁷Cs inventories in the watershed and canal reservoirs (Snidvongs et al. 1995).

The Honolulu watershed was divided into nine segments with one rain gauge station representing each of these segments (Figure 8, Table 6). Fallout from nuclear testing has traditionally been measured using the activity of ⁹⁰Sr, a nuclear fission product with $t_{1/2} = 28.8 \text{ yr}$, as a proxy nuclide (HASL 1977). For our model, ⁹⁰Sr fallout into a segment i is assumed to observe the relationship:

$$F_i = \alpha C_A (1 - e^{-\gamma P_i}) \quad (7)$$

(Robbins 1985), where $F_i = ^{90}\text{Sr}$ fallout in $\text{mCi km}^{-2} \text{ month}^{-1}$ (a function of space and time); $C_A =$ atmospheric ⁹⁰Sr concentration (over a short distance, the atmosphere is assumed to be homogeneous and C_A is a

function of time only); P_i = precipitation in cm month^{-1} ; γ = "atmospheric wash-out" kinetic order (nondimensional); and α = an arbitrary constant.

Because αC_A is a function of time but not space, it can be estimated for a given time if the fallout and rainfall records at two or more stations in the same general area are available. The monthly αC_A are calculated by using the ^{90}Sr fallout and rainfall reported for four sites in the Hawaiian Islands by HASL (1977)—Coconut Island (O'ahu), Līhu'e (Kaua'i), Maunalo (Maui), and Hilo (Hawai'i)—between 1960 and 1969 (the only period when the data from these four sites

overlapped). Subsequently, monthly F_i , αC_A , and P_i for these four sites are substituted into equation 7 and the best-fit γ of 0.0103 is obtained (Figure 9). This γ for the Hawaiian Islands is comparable with that of 0.02 found for the Great Lakes region by Robbins (1985).

After the kinetic order (γ) is obtained, the relative fallout between any two locations can be known without knowing the αC_A . For each segment i in the Honolulu watershed as well as for the Ala Wai Canal (Figures 2 and 8), the calculated monthly fallout per unit area (F_i) is linked to the fallout observed at the Hawai'i Institute of Marine Biology

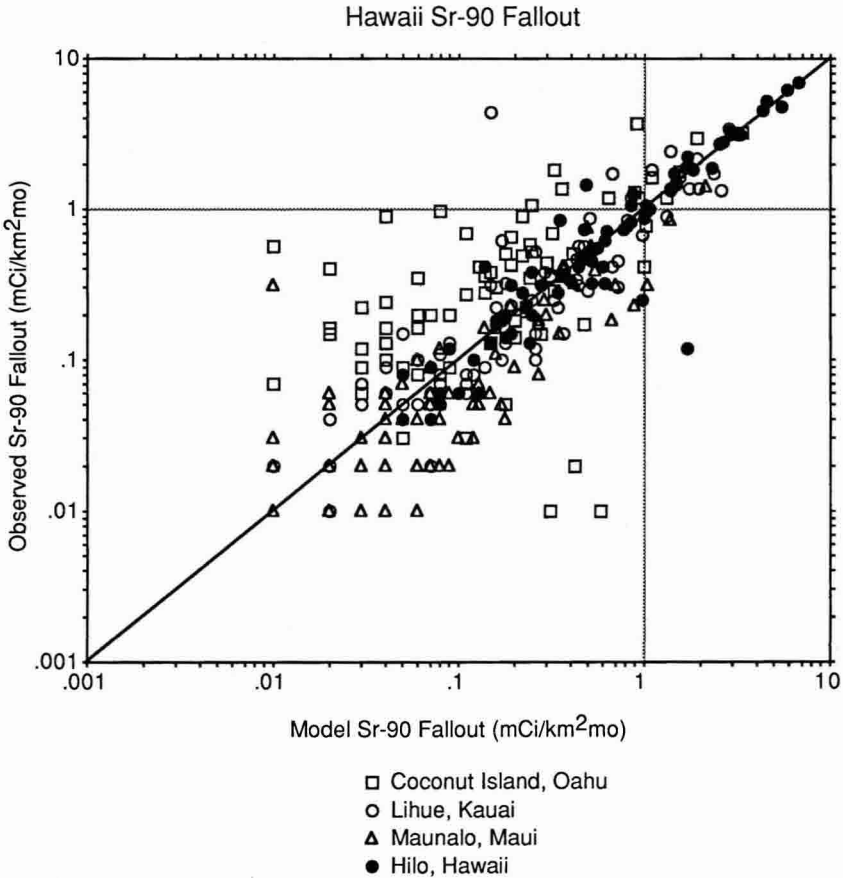


FIGURE 9. Comparison between observed ^{90}Sr fallout at four Hawai'i stations (Coconut Island, O'ahu; Līhu'e, Kaua'i; Maunalo, Maui; and Hilo, Hawai'i) and ^{90}Sr fallout predicted by equation 5 for $\gamma = 0.0103$ (see text for explanation). Data from HASL (1977).

(HIMB, formerly the Hawaiian Marine Laboratory) on Coconut Island, windward O'ahu (F_{CI}), i.e.:

$$F_i = F_{CI} \quad (8)$$

Artificial radionuclide fallout is assumed to have occurred mainly between May 1957 and September 1974. Missing monthly fallout data at HIMB during that period were linearly interpolated. Fallout after September 1974, if there was any, would have been very small in Hawai'i and is neglected in this study. The total fallout of ^{90}Sr into each watershed and canal segment was obtained by multiplying F_i by the segment area (Table 6). The fallout of ^{137}Cs is converted from ^{90}Sr using the $^{137}\text{Cs}:^{90}\text{Sr}$ fallout activity ratio of 1.5 (e.g., Ritchie and McHenry 1990). One further assumption of the model is that there is no loss of ^{137}Cs from the canal-watershed system except by radioactive decay, but ^{137}Cs is allowed to relocate from

the watershed soil to the canal sediment by soil erosion.

The net ^{137}Cs input into the canal sediments (watershed erosion plus direct atmospheric fallout) is modeled by two nonsteady-state mass-balance equations (Snidvongs et al. 1995):

$$\frac{dM_i}{dt} = F_i - (k \cdot P_i^n + \lambda)M_i \quad (9)$$

for the watershed segment i (in this study $i = 1$ to 9), and:

$$\frac{dM_c}{dt} = F_c - \lambda M_c + k \cdot \sum_{i=1}^9 [P_i^n M_i] \quad (10)$$

for the canal sediments, where P_i = rainfall in cm month^{-1} into segment c ; M_i and M_c = ^{137}Cs inventories (in mCi) in watershed segment i and in canal segment c , respectively; k = empirical erosion coefficient (month cm^{-2}); n = erosion kinetic order with respect

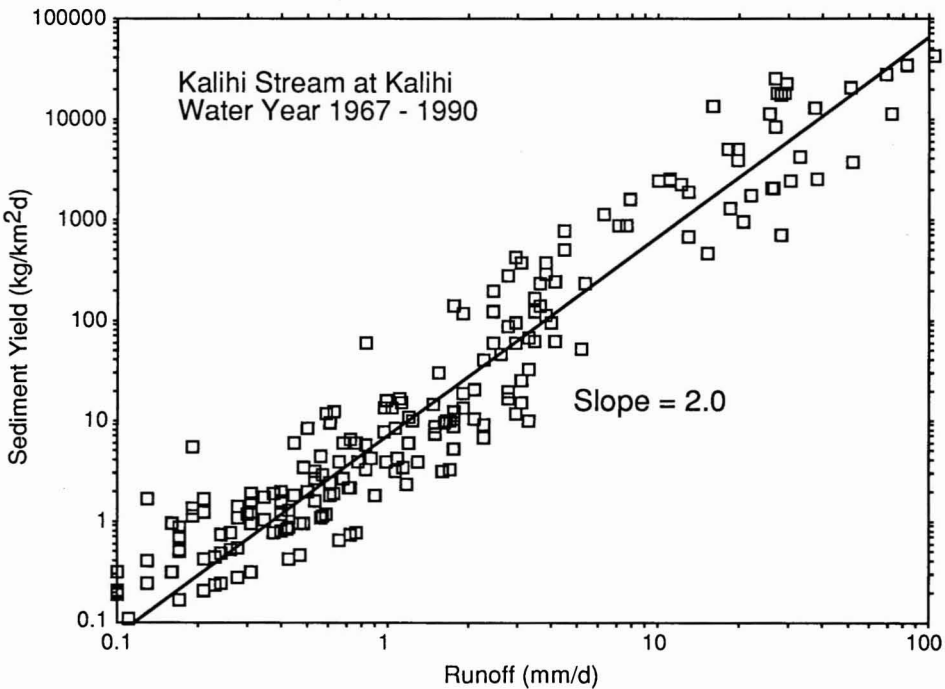


FIGURE 10. Sediment rating curve for Kalihi Stream, leeward O'ahu, based on data from 1967 to 1990. The log-log slope of 2.0 is estimated from an eye fit of the data. Data from U.S. Geological Survey (1967-1990).

to rainfall; and $\lambda = {}^{137}\text{Cs}$ radioactive decay constant ($0.00192 \text{ month}^{-1}$).

In this study, n was estimated based on the discharge rate and suspended solid concentration measured in Kalihi Stream (watershed area = 13.42 km^2), the only stream in the vicinity of Honolulu for which long-term data are available (U.S. Geological Survey 1967–1990). The plot between the logarithms of stream runoff and sediment yield (Figure 10) reveals that the data could possibly be fitted by a slope of 2. If runoff is correlated linearly with rainfall (a reasonable assumption for small watersheds on the island where stream flow responds to rainfall almost

instantly), there is an implication that erosion (sediment yield) is also a square function of rainfall (i.e., $n = 2$).

The total ${}^{137}\text{Cs}$ inventory in the Ala Wai Canal sediments at the July 1991 collection date in each of the three segments of the canal (Figure 2)—inner (G-8), middle (M-21), and outer (M-3)—was estimated by multiplying the segment area with the specific activity per unit area obtained from each representative core (Table 6, Figure 7). The total ${}^{137}\text{Cs}$ inventory in the Ala Wai Canal sediments (M_c , July 1991) is calculated to be 59.43 mCi (inventory ratio among inner: middle: outer zones = $0.07:0.80:0.13$).

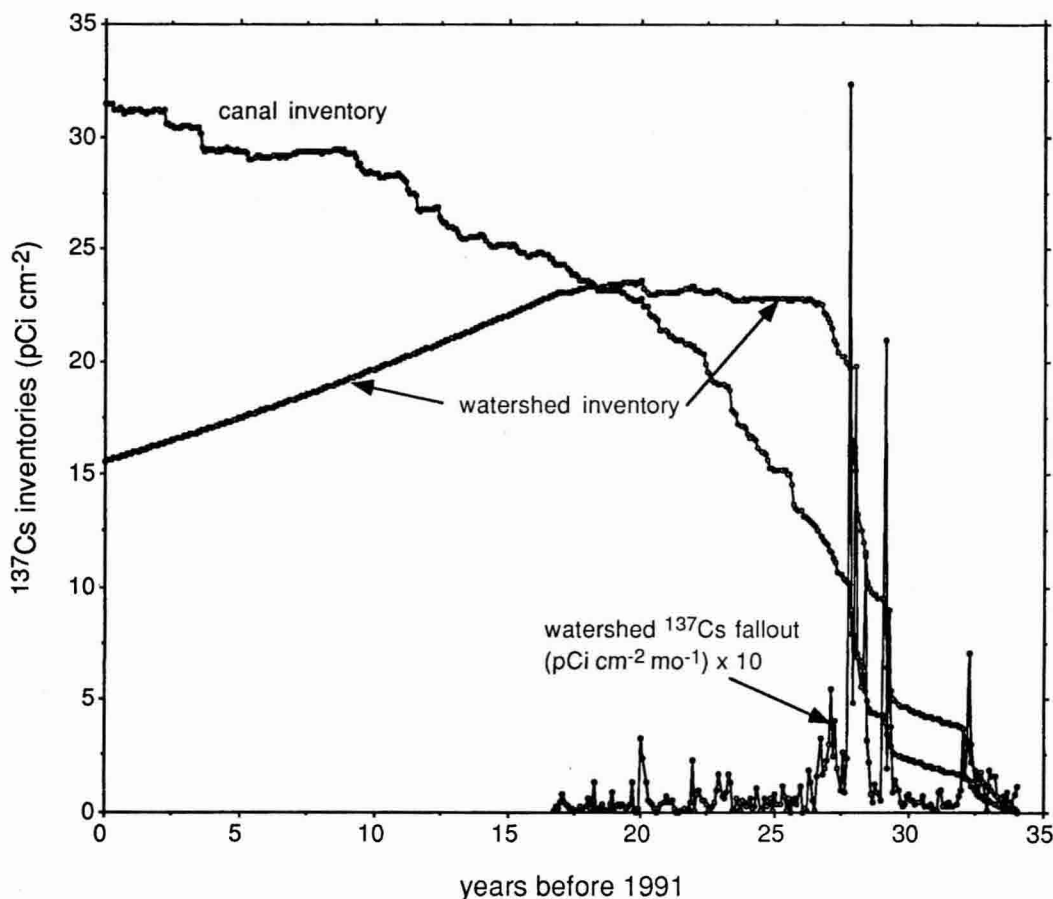


FIGURE 11. Time series of watershed soil and Ala Wai Canal sediment inventories predicted by the nonsteady-state two-box model for ${}^{137}\text{Cs}$ (equations 9 and 10). Also shown is the time series of ${}^{137}\text{Cs}$ deposition estimated for the watershed from Hawaii's ${}^{90}\text{Sr}$ fallout records.

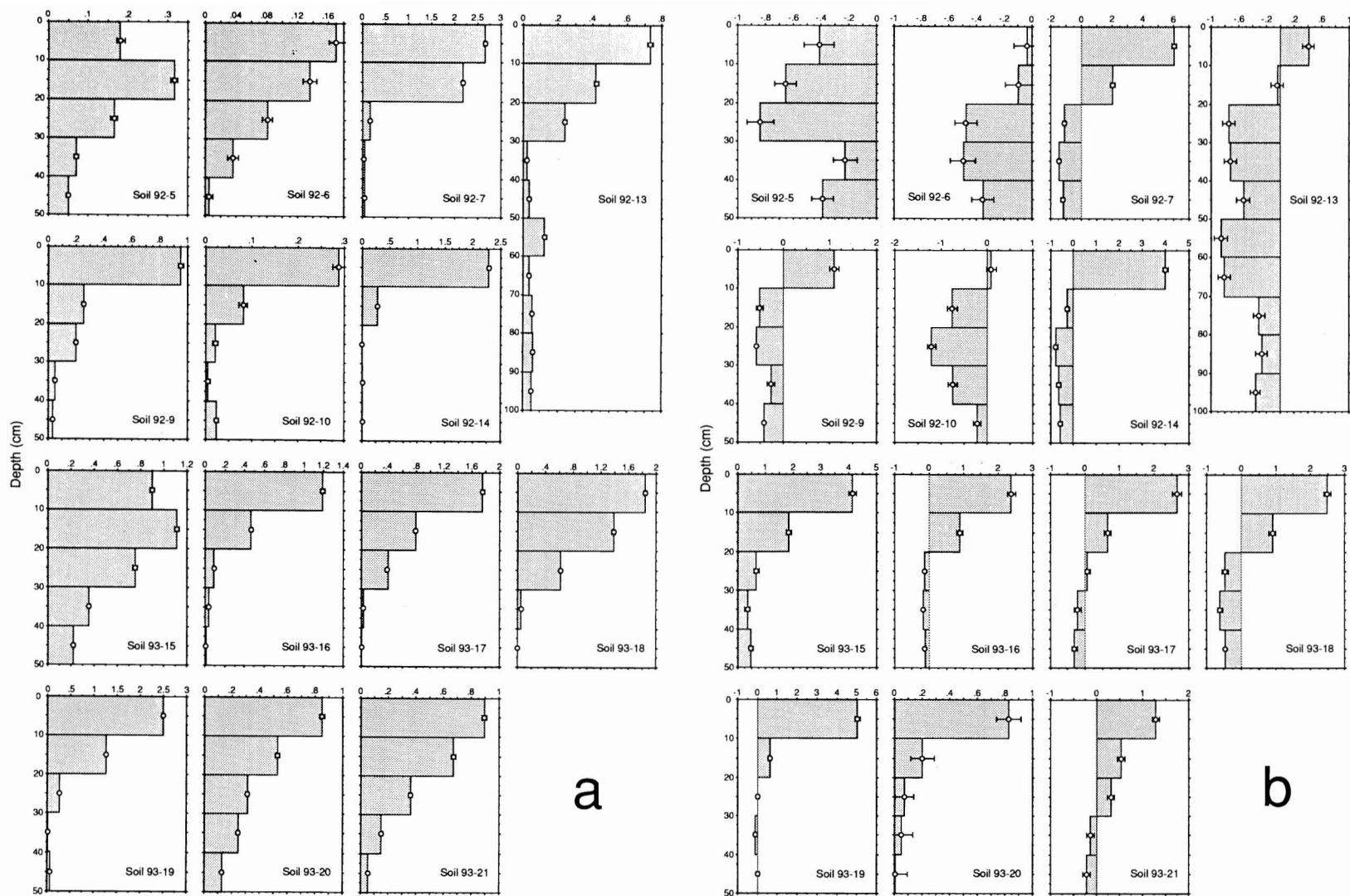


FIGURE 12. (a) Depth distribution of ^{137}Cs activity for central Honolulu watershed soils. (b) Depth distribution of excess ^{210}Pb activity for central Honolulu watershed soils.

By solving equations 9 and 10 with this 59.43 mCi boundary value for M_c , the k value of 2.703×10^{-8} month cm^{-2} is obtained. By substituting this k into equation 9, it is also possible to predict the soil ^{137}Cs inventory for each watershed segment (Table 6). Figure 11 shows the changes with time of the total watershed and canal ^{137}Cs inventories predicted by equations 9 and 10 with the 59.43 mCi boundary value for M_c . As expected, the watershed inventory that built up quickly in the mid-1950s to mid-1960s has subsequently plateaued and decreased owing to diminished fallout, radioactive decay, and soil erosion. In contrast, the canal sediment inventory has continued to build as it receives ^{137}Cs from the watershed soils. For this system, the time-dependent input for the fluvial-marine system is <100 times the size of the time-dependent input for the watershed (i.e., ^{137}Cs sedimentation in the Ala Wai Canal is dominated by soil erosion, and transport through the watershed is rapid).

Measured profiles of soil ^{137}Cs and excess

^{210}Pb activities for 14 watershed sites are presented in Figure 12. Inspection of Figure 12 shows that ^{137}Cs penetrates only a short distance into the soil; most soil profiles have only trace amounts of ^{137}Cs below depths of about 30 cm. Excess ^{210}Pb activities are also greatest in the uppermost 20 cm of the profile. Most soils show the effects of ^{222}Rn diffusion in the lower portions of the profile, and it is unclear what proportion of the excess ^{210}Pb in the upper portions is attributable to direct fallout versus ^{222}Rn diffusion and possible retention in the upper, relatively moist, organic matter-rich zone (Table 1).

A comparison between model-predicted and observed soil ^{137}Cs activities is shown in Figure 13. Most of the soil activities cluster around the 1:1 line, with the prominent exception of soil profile no. 16, which was taken from the side of a relatively steep slope where enhanced erosion may have removed the uppermost, ^{137}Cs -enriched soil (see Figure 12a). The agreement between measured and predicted soil ^{137}Cs activities is remarkable con-

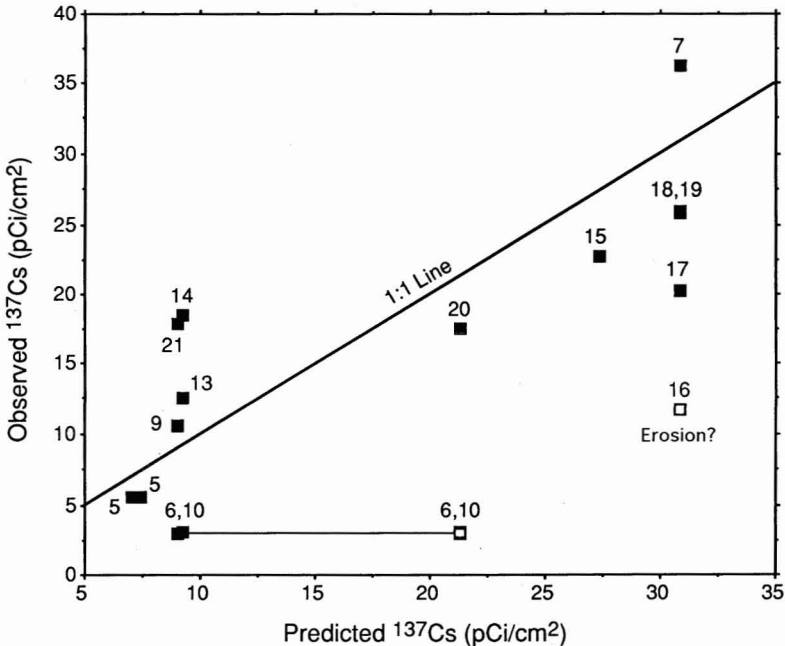


FIGURE 13. Comparison between the observed inventory of ^{137}Cs in watershed soils and the inventory predicted for July 1991 by mass-balance model equation 7 for the corresponding watershed segments (Table 6). Two predicted values are given for soil profiles 6 and 10 because of their location near segment borders (Figures 1 and 8).

sidering the well-known heterogeneity of island rainfall and the relatively small size of the data set. This agreement indicates that most of the ^{137}Cs eroded from the central Honolulu watershed is collected by the canal sediments and supports the validity of the erosion/redeposition model.

Because no substantial bioturbation or other sediment mixing mechanisms (e.g., slumps) were observed in these three cores and considerable ^{137}Cs diffusion is unlikely for these sediments, each individual section in the core can be "dated" by comparing the ^{137}Cs activity in the section with the decay-corrected monthly ^{137}Cs input. For example, if the activity in the topmost 4-cm section of a core is x pCi cm^{-2} , the decay-corrected monthly input is summed from July 1991 backward month by month until x pCi cm^{-2} (or the nearest estimate) is obtained. This summation gives the time interval in months when the topmost section was deposited. The computation is repeated for subsequent sections.

Calculated fallout ^{137}Cs sediment age versus downcore depth is shown in Figure 14. For core G-8, the average sedimentation rate is 2.5 cm/yr from the surface to about 80 cm depth, with a relatively rapid rate of about 22 cm/yr between 80 and 120 cm. The more shallow ^{137}Cs sedimentation rate is comparable with the average rate of 2.4 cm/yr between ca. 20 and 120 cm indicated by the constant flux excess ^{210}Pb model; however, the constant flux excess ^{210}Pb model suggests no rapid sedimentation rate between 80 and 120 cm and predicts a slower rate below that depth (cf. Figures 6 and 14). Extrapolation of the 2.5 cm/yr average rate below 120 cm (where the practical dating limit of about 35 years B.P. for this method has been reached in this core) yields a date of 1933 for the 200-cm base of the G-8 core, in line with an estimated age of about 1927 for the canal. For core M-21, the average ^{137}Cs sedimentation rate is ca. 10 cm/yr from the surface to about a 40-cm depth, followed by an average rate of 4.2 cm/yr from 40 cm to the base of the core at 164 cm. Here, neither excess ^{210}Pb model agrees to within a factor of 2 with the slowest ^{137}Cs sedimentation rate, although the con-

stant activity model predicts a very fast, but undetermined rate from 0 to 40 cm followed by a slow rate (Figure 6). Core M-3 displays three average ^{137}Cs sedimentation rates—fast, slow, fast—of 5.2 cm/yr from 0 to ca. 20 cm, 1.8 cm/yr from 20 to ca. 65 cm, and 10 cm/yr from ca. 65 cm to the core base at 90 cm. Comparison with the excess ^{210}Pb model rates again shows average values that are at least a factor of 2 slower than those of the ^{137}Cs model. Although the constant flux excess ^{210}Pb model generally gives faster rates that are closer to the ^{137}Cs model rates in the upper portions of the cores, it is interesting that the constant activity model predicts rate changes that are generally more in line with the ^{137}Cs model (compare Figures 6 and 14).

It is also possible to calculate the sedimentation rate for each individual section from the results in Figure 14. The results (in $\text{g cm}^{-2} \text{ month}^{-1}$) are plotted against time in Figure 15. Smoothing of these individual sedimentation rates for each core reveals two and possibly three episodes of relatively high sediment accumulation in the canal over the ca. 35-yr period from 1991: 1957–1967, 1979–1982, and 1986–1991. Comparison with the climatic data for Honolulu (compiled in Glenn et al. 1995) shows that the 1957–1967 episode coincides with a dry period from about 1958 to 1962, followed by a wet period from 1962 to 1973 (with the highest rainfall actually ending in about 1968). Although dry, the accumulation rates of marine authigenic phases (organic carbon and calcium carbonate) are quite high during the 1958–1962 period, which marks the beginning of a long-term increase in mean annual temperature. The high sediment accumulation episode from 1979 to 1982 that appears in the G-8 and M-21 cores correlates with a brief period of relatively high rainfall from 1981 to 1982 and again precedes this high rainfall period by a few dry years when the accumulation rates of marine authigenic phases are high. The high sediment accumulation episode from 1986 to 1991 does not appear to coincide with high rainfall, although the annual rainfall trend has increased toward 1990 from a low in 1983.

The lack of an obvious climatic control

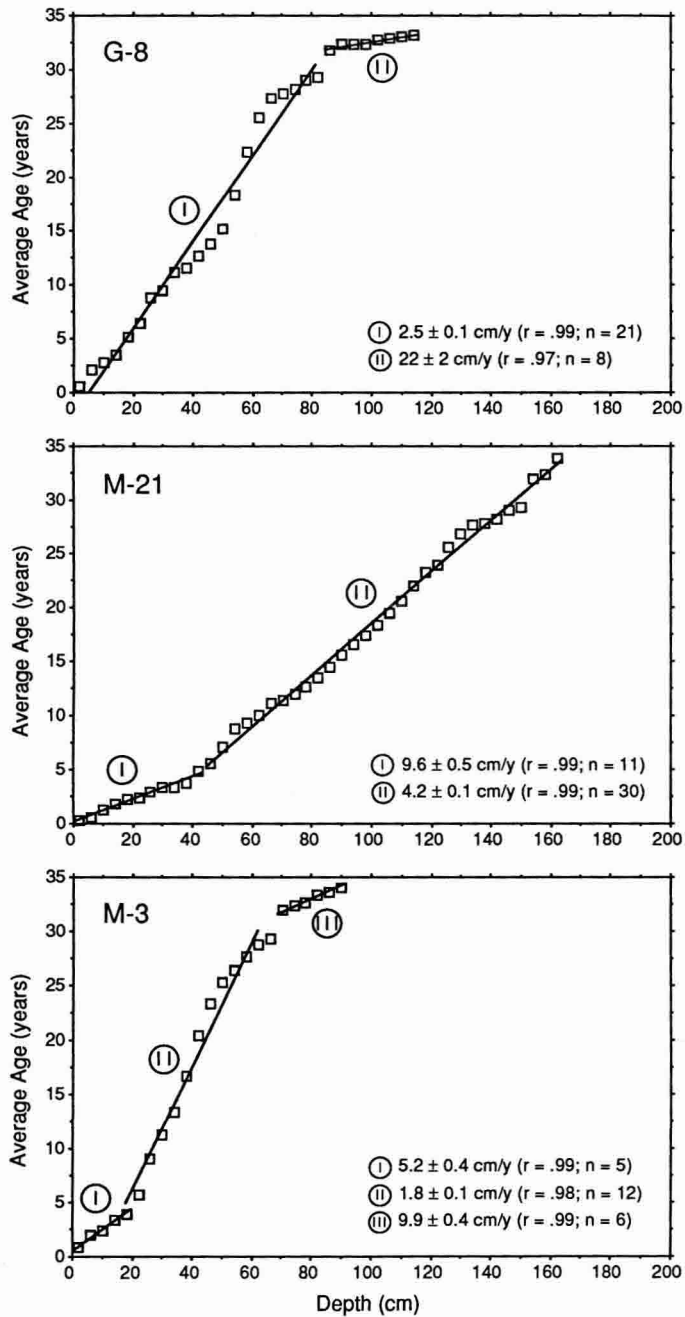


FIGURE 14. ^{137}Cs model-based sediment age versus depth for Ala Wai Canal cores. ^{137}Cs model sedimentation rates are derived from model I regression fits to the more obvious slope changes. Uncertainties are minimum values based solely on the standard error of the regression.

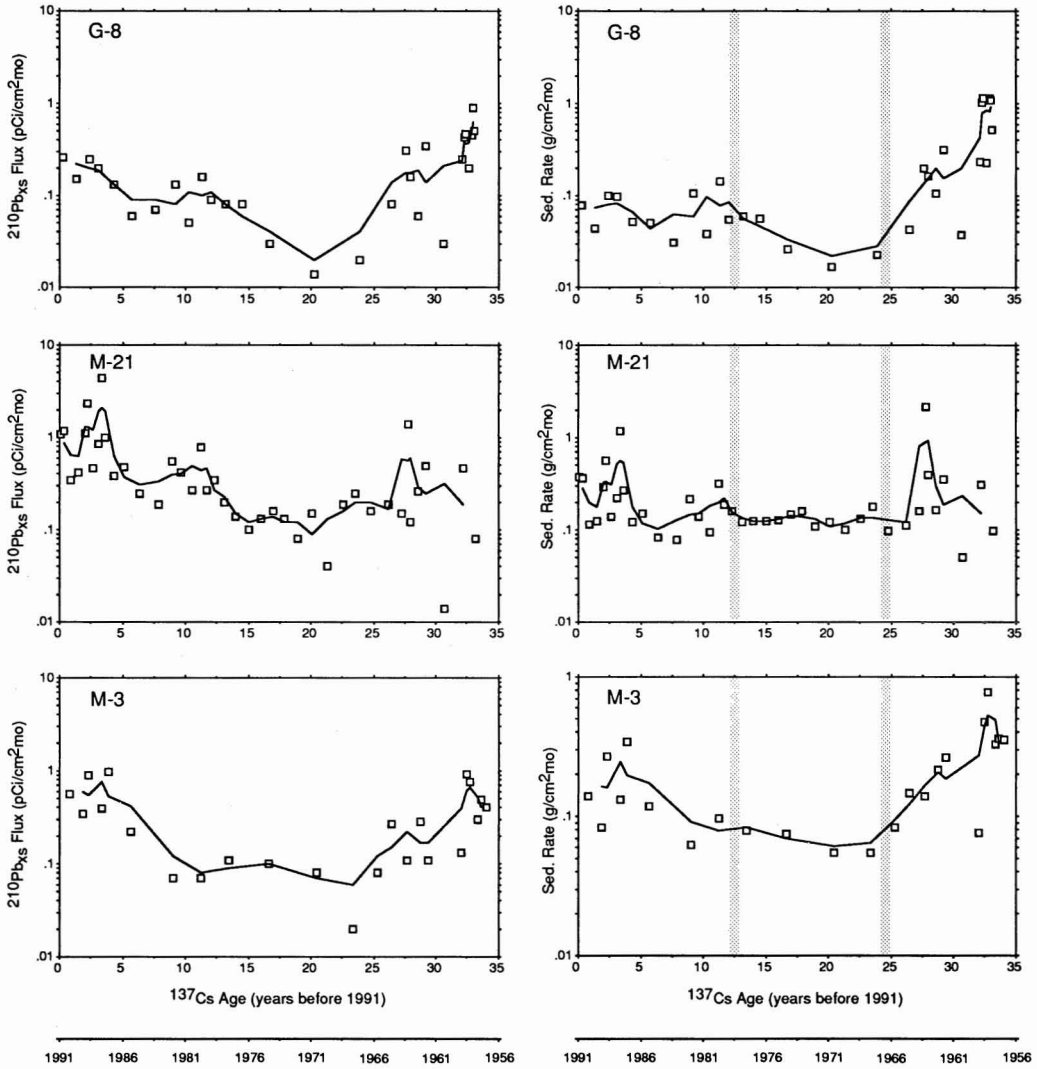


FIGURE 15. Left column: Predicted net flux of excess ^{210}Pb into the Ala Wai Canal sediment cores versus ^{137}Cs model-based sediment age. Right column: ^{137}Cs model-based sedimentation rate versus sediment age. Curve fits are three-point running means. Shaded bars represent silt dredging in 1966 and 1978.

for the most recent high sedimentation episode could invoke anthropogenic causes of increased runoff and erosion since 1986. Although plausible, such causes should be viewed with caution until correlations with known changes in urbanization activity are found. Since 1950, Honolulu's population has grown by 238%, with the largest growth between 1960 and 1970 (114%); between

1980 and 1990, population growth continued at a more modest 10% increase (U.S. Bureau of the Census 1991). The greatest impact upon runoff and erosion probably results from development near the backs of the valleys where topography is steepest and rainfall is highest, a scenario supported by the watershed distributions of ^{137}Cs and excess ^{210}Pb (Figures 1 and 12, Table 6) and the generally

high activities of these radionuclides in the $<45 \mu\text{m}$ fraction of the stream sediments (Table 5). Since 1986, urban development within the central Honolulu watershed has, however, been primarily in relatively low-relief areas of the coastal plain. Other potential causes are changes in land use and protective vegetation in the steeper and wetter portions of the watershed.

The two sill dredging events, in 1966 and 1978–1979, coincide with the end and the beginning of the 1957–1967 and 1979–1982 high sediment accumulation periods, respectively (Figures 2 and 15). Changes in sediment accumulation by redistribution of bulk sediment into other portions of the canal during dredging are possible, but should be relatively instantaneous. Longer-term changes in the marine authigenic accumulation show no correlation with the 1966 sill dredging, although a case could be made for the dredging in 1978–1979 (Glenn et al. 1995). In addition, there is no evidence of such instantaneous events in the core lithology (Glenn et al. 1995) nor of large shifts in the sediment excess ^{210}Pb activity profiles that would result from sedimentation of older material (downward for excess ^{210}Pb). Upward or downward shifts for ^{137}Cs would be expected, depending on the age of the sediment redistributed. There is evidence for a correlation of some of the ^{137}Cs peaks in Figure 7 with the two dredging events. However, we ascribe this correlation more to coincidence with the watershed fallout depositional record, because we would not expect to find consistently high activities associated with redistributed sediments and there are other observed ^{137}Cs activity peaks in the profiles that do not correlate with the two events (compare Figures 7 and 15). There is also little evidence for a consistent pattern of sedimentation in the canal before and after the sill dredging events (Figure 15).

Implications for Watershed Erosion and Canal Sedimentation

Using the ^{137}Cs model-based mass accumulation rates, canal segment areas, and mean dry bulk densities for the three canal

cores (from Table 1), we estimate mean sedimentation rates over the period 1957–1991 of 1.1 ± 0.2 , 5.4 ± 1.0 , and $1.0 \pm 0.3 \times 10^3 \text{ m}^3 \text{ yr}^{-1}$ for the outer, middle, and inner Ala Wai Canal segments, respectively (Figure 2, Table 6). Based on changes in bathymetry during the 40 months following the canal dredging in 1966, Gonzalez (1971) estimated a mean sedimentation rate for the canal of $7 \times 10^3 \text{ m}^3 \text{ yr}^{-1}$. More recently, Laws et al. (1993) estimated a similar mean sedimentation rate for the canal of $8 \times 10^3 \text{ m}^3 \text{ yr}^{-1}$ based on bathymetry changes since the 1978–1979 dredging and surveys conducted in 1991. Our estimate of $5.4 \pm 1.0 \times 10^3 \text{ m}^3 \text{ yr}^{-1}$ for the middle canal segment is comparable with but slightly lower than the Gonzalez and Laws et al. estimates based on changes in the sill depth between the Mānoa-Pālolo Stream drainage canal and the McCully Street bridge (Figure 2), where canal sedimentation is greatest (Gonzalez 1971).

For each canal segment, we calculate mean bulk sediment accumulation rates of 619, 2156, and 323 metric tons yr^{-1} for the outer, middle, and inner canal segments, respectively. Using the detrital fractions for each core, the mean detrital sediment accumulation rates are 514, 1848, and 264 metric tons yr^{-1} , respectively. The total mean bulk sediment accumulation rate for the canal is 3098 tons yr^{-1} , with 2626 tons yr^{-1} accumulation of detrital phases and 472 tons yr^{-1} accumulation of authigenic marine phases. The sediment yield for the central Honolulu watershed is $61.2 \text{ tons km}^{-2} \text{ yr}^{-1}$, based on the detrital sediment accumulation rates and assuming no sediment loss from the canal. The detrital sediment accumulation in the Ala Wai Canal is $13,900 \text{ tons km}^{-2} \text{ yr}^{-1}$, yielding a watershed-to-canal focusing factor of about 230. The sediment yield value can be translated into a physical denudation rate of $5.55 \text{ mg cm}^{-2} \text{ yr}^{-1}$ for the central Honolulu watershed, which is at the low end of the range of physical denudation rate estimates for O'ahu of $6\text{--}30 \text{ mg cm}^{-2} \text{ yr}^{-1}$ (Li 1988). Typically, chemical denudation is 50% of the total denudation rate in relatively low runoff areas in Hawai'i and about 30% of the total rate in relatively high runoff areas (Li 1988).

Therefore, the total denudation rate for the relatively dry, leeward-facing central Honolulu watershed is probably about $12 \text{ mg cm}^{-2} \text{ yr}^{-1}$, as compared with a total estimate based on Ca leaching rates for the relatively wet, windward-facing Kāneʻohe Bay watershed of $34 \text{ mg cm}^{-2} \text{ yr}^{-1}$ (Moberly 1963).

Estuaries are ephemeral features whose geological lifetimes are comparatively short (Kennett 1982). Using an average canal water depth of 2 m estimated by Gonzalez in 1971 as a reasonable maximum depth for the canal in 1991, after the 1978–1979 dredging and reestablishment of the sill, we have estimated the times required to fill the canal at the mean sedimentation rates for the 1957–1991 period. These are 74, 41, and 72 yr for the outer, middle, and inner canal segments, respectively. The average time to fill the entire canal is 62 yr, assuming that little sediment escapes the canal. Clearly, continued maintenance of the Ala Wai Canal will require periodic dredging, not only to improve circulation and water quality, but also to keep the area from returning to its former wetlands state.

Implications for Excess ^{210}Pb Flux

With all sections in the three cores dated, the excess ^{210}Pb flux into the canal sediments at the time when each section was deposited can be estimated. Our ^{137}Cs model-predicted flux of excess ^{210}Pb into each canal segment during the past ca. 35 yr from July 1991 is shown in Figure 15. The flux is clearly not constant over time and generally follows the sedimentation rate, indicating that soil erosion is probably the major source of excess ^{210}Pb for the Ala Wai Canal sediments. However, when the two variables are plotted against each other (Figure 16), more than 50% of the data deviate from a linear relationship (i.e., the log-log slope of 1) toward higher excess ^{210}Pb fluxes, which suggests that there may be some other pathway(s) of excess ^{210}Pb input superimposed upon soil erosion.

There are three possible sources for the atmospheric deposition of excess ^{210}Pb in the Hawaiian Islands: ^{222}Rn degassing of island soils and rocks, air transported to Hawai'i

from continental areas, and gas emissions from active volcanism on the island of Hawai'i. Maritime air is not considered an important source of parental ^{222}Rn emission (Turekian et al. 1977). Of these three possible sources, continental air (Larson 1974) and volcanic emissions are considered more important sources of excess ^{210}Pb input to the Hawaiian Islands.

A case can be made for atmospheric deposition of excess ^{210}Pb from volcanic emissions during active Hawaiian volcanism. Figure 17 shows episodes of intense fire-fountaining of Kīlauea Volcano along with the temporal variations of the excess ^{210}Pb flux. There appear to be 3- to 5-yr time lags between these episodes and peaks in the excess ^{210}Pb flux. These time lags agree with estimates of 3- to 5-yr mean transit times based on watershed models of ^{137}Cs , ^{210}Pb , and Pu isotopes (Smith et al. 1987). The association of increased ground radon concentrations with Kīlauea eruptive and seismic activity (Cox et al. 1980, Thomas et al. 1986) and increased radon emission from hot springs and fumaroles with volcanism elsewhere (Chirkov 1975, Hauksson 1981a) suggest a mechanism of enhanced ^{222}Rn flushing through pore fluids by magmatic temperature and pressure (Gasparini and Mantovani 1978), fissure closing (Hauksson 1981a), and slow crack growth in rock associated with stress corrosion (Hauksson 1981b). Direct magmatic degassing may also be important, especially in the early, intense fire-fountaining stages, but little eruptive-plume ^{222}Rn data exist, especially for Hawaiian volcanoes. Larson (1974) found no enhanced ^{222}Rn concentrations in air samples collected in the plume of Kīlauea Volcano during 1 day of the Mauna Ulu eruption in 1972, but few samples (three) were collected, and temporal variability in volcanic ^{222}Rn emission was not addressed.

Larson (1974) and, more recently, Hutter et al. (1994) reported elevated ^{222}Rn concentrations in air masses over the Hawaiian Islands that appear to originate from continental areas. Continuous measurements of atmospheric ^{222}Rn for the past 2 yr at the Mauna Loa Observatory on the island of

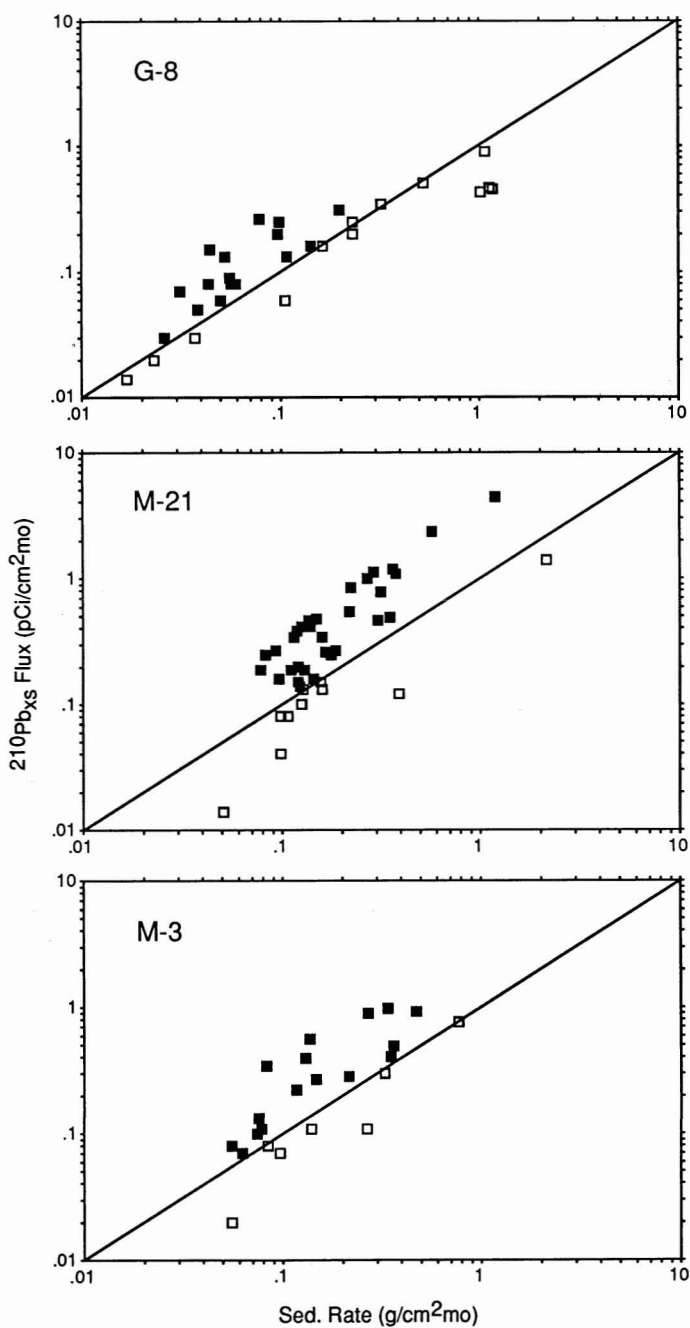


FIGURE 16. Predicted net flux of excess ^{210}Pb versus ^{137}Cs model-based sedimentation rate. Solid squares lie above the 1 : 1 line; open squares lie on or below the 1 : 1 line.

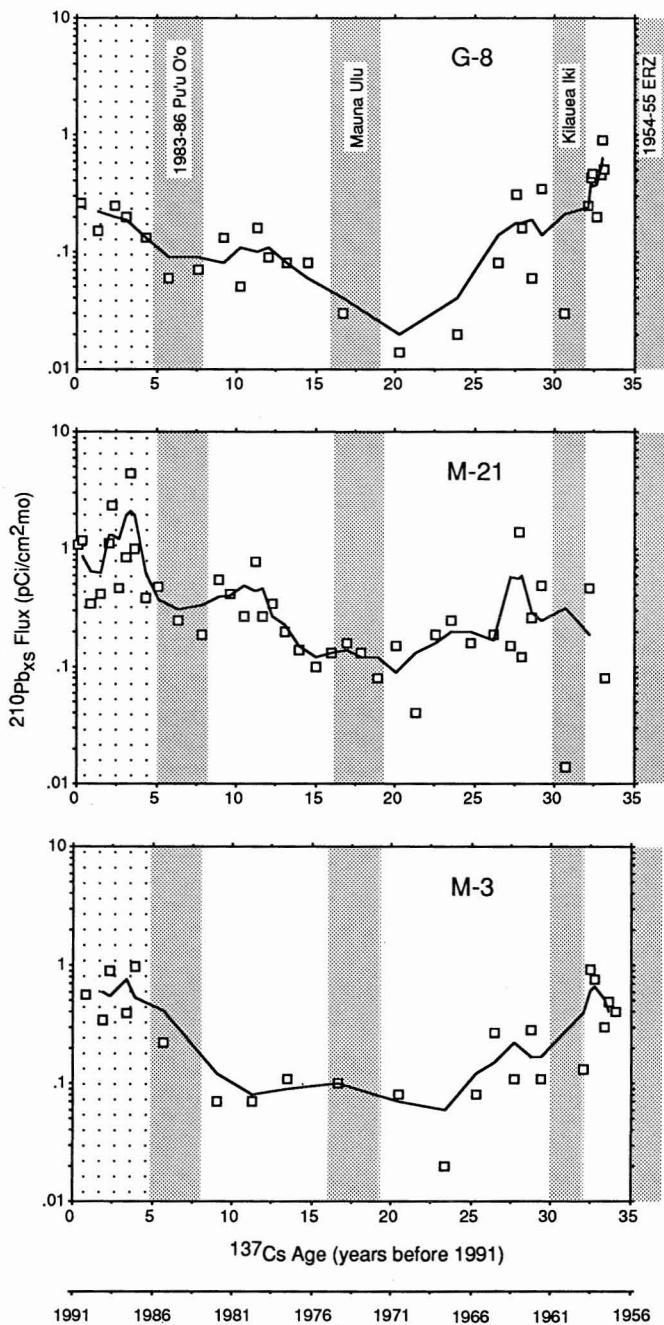


FIGURE 17. Predicted net flux of excess ^{210}Pb into the Ala Wai Canal sediment cores versus ^{137}Cs model-based sediment age, superimposed with phases of intense fire-fountaining of Kīlauea Volcano (fine shading). Coarse shading indicates low-intensity fire-fountaining of Pu'u Ō'ō vent eruption subsequent to 1986. ERZ = East Rift Zone. Eruption data compiled from Tilling et al. (1987) and Tilling and Dvorak (1993).

Hawai'i reveal that springtime maximum values (> 100 times fall values) are associated with distal transport in the lower troposphere from the Asian continent (Hutter et al. 1994). Therefore, variations in the deposition of excess ^{210}Pb may correspond with periods of more frequent or more rapid transport of ^{222}Rn -laden air from Asia, especially if coincident with excessive precipitation.

The variation in the excess ^{210}Pb flux into the canal sediments could be related to the mechanism of soil erosion. This relation is suggested by a comparison of the excess ^{210}Pb inventories for cores G-8, M-21, and M-3 of 28, 82, and 41 pCi cm^{-2} , respectively, with the ^{137}Cs inventories for these cores listed in Table 6. The relative proportions of the inventories for both nuclides are nearly identical. Figure 12*b* shows that the soil activities of excess ^{210}Pb are greatest in the shallowest portions of the profile, and that excess ^{210}Pb activities, like those of ^{137}Cs (Figure 12*a*), are greatest in soils from wet watershed locations near the back of the valleys (Figure 1). The latter enrichment is primarily a function of rainfall, but for excess ^{210}Pb , this enrichment is also a result of decreased ^{222}Rn degassing in more perennially water-saturated soils. If rainfall patterns within the watershed vary broadly over time so that during more intense rainfall periods increased erosion and transport of excess ^{210}Pb -rich top soils from the back of the valleys occur, then perhaps the temporal variation in excess ^{210}Pb flux is simply reflecting a watershed process.

CONCLUSIONS

Despite derived sedimentation rates for the Ala Wai Canal sediments that are reasonable when compared with those of other estuarine and coastal sites, both the constant flux or constant activity models of excess ^{210}Pb geochronology are inconsistent with the known age of the Ala Wai Canal. Geochronology based on a ^{137}Cs erosion/redeposition model yields sedimentation rates for the canal that generally exceed those based upon excess ^{210}Pb by more than a factor of two and are in

agreement with the known age of the canal and with sedimentation rate estimates based upon bathymetry changes.

The Ala Wai Canal collects bulk sediment at a mean rate of about 3100 tons annually. About 80% of the sediment is detrital clays from erosion of the central Honolulu watershed, whereas about 20% of the sediment is composed of marine authigenic and biogenous phases (carbonates, organic matter, sulfides, and siliceous tests). The sediment yield for the central Honolulu watershed of about 60 metric tons $\text{km}^{-2} \text{yr}^{-1}$ equates to a physical denudation rate of ca. 6 $\text{mg cm}^{-2} \text{yr}^{-1}$, which is at the low end of the range of physical denudation rate estimates for the island of O'ahu; however, watershed-to-canal sediment focusing is high. Based on the mean ^{137}Cs sedimentation rates and an average canal water depth of 2 m, the average time to completely fill the canal is about 60 yr, assuming that little sediment escapes. The mean fill time is only about 40 yr for the middle canal segment, which receives most of the silt development from the Mānoa-Pālolo Stream drainage canal, whereas for the outer and inner canal sediments, the mean fill times are about 70 yr. Periodic dredging of the canal, especially of the middle segment, is clearly indicated.

Fallout ^{137}Cs -derived sedimentation rates for each canal core reveal two and possibly three episodes of relatively high sediment accumulation in the canal over the ca. 35-yr period before 1991: 1957–1967, 1979–1982, and 1986–1991. The two earlier episodes appear to coincide with periods of high rainfall, but are generally preceded by dry periods where accumulation of marine authigenic phases are high. The most recent high sediment accumulation episode does not appear to correlate with high rainfall, although the annual rainfall trend has increased toward 1990 from a low in 1983. There is little evidence for impacts upon sediment accumulation in canal areas not directly affected by the sill dredging in 1966 and 1978–1979 or for a consistent pattern of sedimentation in the canal before and after the sill dredging.

For the Ala Wai Canal, the flux of excess ^{210}Pb follows the sedimentation rate and is

clearly not constant with time. Moreover, from the relationship between the excess ^{210}Pb flux and sediment accumulation, the specific activity of the sediment arriving in the canal also is not constant with time. Perhaps a nonsteady-state model could be developed for excess ^{210}Pb similar to that used for fallout ^{137}Cs , but such a model would also have to account for nonconstant specific activity of the eroding and depositing sediments. Of the possible reasons for higher excess ^{210}Pb fluxes than those expected from a linear relationship, nonsteady-state atmospheric input to the Hawaiian Islands from ^{222}Rn -rich air masses that originate in Asia currently appears more plausible than ^{222}Rn emissions from Hawaiian volcanism. Both of these potential sources should be further evaluated with more data. Variations of the excess ^{210}Pb flux into the canal sediments may, however, simply be related to a not-so-simple mechanism of soil erosion.

ACKNOWLEDGMENTS

We thank Eric De Carlo, Jason Tan, and the students of the NSF Young Scholars Program, in particular Brook Maples, Douglas McCrath, Patrick Unemori, Clayton Yeung, Melanie Shiraki, and Billy Kang, for their assistance in sample collection and processing. The Commission on Water Resource Management, Department of Land and Natural Resources, State of Hawai'i, kindly supplied rainfall data for the Honolulu watershed. Brooks Bays of SOEST Illustration provided outstanding technical support and personally verified the location of Makiki Stream. An early version of the manuscript was improved by helpful reviews of Y.-H. Li and an anonymous reviewer. We also thank Barbara Jones for editorial assistance and J. M. Resig for editorial handling of the manuscript.

LITERATURE CITED

- BERNER, R. A. 1980. Early diagenesis: A theoretical approach. Princeton University Press, Princeton, New Jersey.
- CARTER, M. W., and A. A. MOGHISSI. 1977. Three decades of nuclear testing. *Health Phys.* 33:55–71.
- CHIRKOV, A. M. 1975. Radon as a possible criterion for predicting eruptions as observed at Karymsky volcano. *Bull. Volcanol.* 37:126–131.
- COX, M. E., K. E. CUFF, and D. M. THOMAS. 1980. Variations in ground radon concentrations with activity of Kilauea Volcano, Hawaii. *Nature (Lond.)* 288:74–76.
- DE CARLO, E. H., and K. J. SPENCER. 1995. Records of lead and other heavy metal inputs to sediments of the Ala Wai Canal, O'ahu, Hawai'i. *Pac. Sci.* 49:471–491.
- EDGINGTON, D. N., J. VAL KLUMP, J. A. ROBBINS, Y. S. KUSNER, V. D. PAMPURA, and I. V. SANDIMIROV. 1991. Sedimentation rates, residence times and radionuclide inventories in Lake Baikal from ^{137}Cs and ^{210}Pb in sediment cores. *Nature (Lond.)* 350:601–604.
- FRYER, P. 1995. The 1991–1992 NSF Young Scholars Program at the University of Hawai'i: Science and engineering studies of the Ala Wai Canal, an urban estuary in Honolulu. *Pac. Sci.* 49:319–331.
- GASPARINI, P., and M. S. M. MANTOVANI. 1978. Radon anomalies and volcanic eruptions. *J. Volcan. Geotherm. Res.* 3:325–341.
- GILLHAM, R. W., J. A. CHERRY, and L. E. LINDSAY. 1980. Cesium distribution coefficients in unconsolidated geological materials. *Health Phys.* 39:637–649.
- GLENN, C. R., and G. M. MCMURTRY. 1995. Scientific studies and history of the Ala Wai Canal, an artificial tropical estuary in Honolulu. *Pac. Sci.* 49:307–318.
- GLENN, C. R., S. RAJAN, G. M. MCMURTRY, and J. BENAMAN. 1995. Geochemistry, mineralogy, and stable isotopic results from Ala Wai estuarine sediments: Records of hypereutrophication and abiotic whittings. *Pac. Sci.* 49:367–399.
- GONZALEZ, F. I., JR. 1971. Descriptive study of the physical oceanography of the Ala Wai Canal. Hawai'i Institute of Geophysics Technical Report HIG-71-7.
- HASL. 1977. Final tabulation of monthly ^{90}Sr fallout data: 1954–1976. U.S. Energy

- Research and Development Administration, Health and Safety Laboratory Report no. HASL-329.
- HAUKSSON, E. 1981*a*. Episodic rifting and volcanism at Krafla in north Iceland: Radon (222) emission from fumaroles near Leirhnjúkur. *J. Geophys. Res.* 86:11,806–11,814.
- . 1981*b*. Radon content of groundwater as earthquake precursor: Evaluation of worldwide data and physical basis. *J. Geophys. Res.* 86:9397–9410.
- HIRSCHBERG, D. J., and J. R. SCHUBEL. 1979. Recent geochemical history of flood deposits in northern Chesapeake Bay. *Estuarine Coastal Mar. Sci.* 9:771–784.
- HUTTER, A. R., R. J. LARSEN, H. MARING, and J. MERRILL. 1994. Radon-222 at Bermuda and Mauna Loa: Local and distant sources. *J. Radioanal. Chem.* (in press).
- KENNETT, J. P. 1982. *Marine geology*. Prentice Hall, Englewood Cliffs, New Jersey.
- KIM, K. H., and W. C. BURNETT. 1983. Gamma-ray spectrometric determination of uranium-series nuclides in marine phosphorites. *Anal. Chem.* 55:1796–1800.
- KIM, K. H., and G. M. MCMURTRY. 1991. Radial growth rates and ^{210}Pb ages of hydrothermal massive sulfides from the Juan de Fuca Ridge. *Earth Planet. Sci. Lett.* 104:299–314.
- KOIDE, M., A. SOUTAR, and E. D. GOLDBERG. 1972. Marine geochronology with ^{210}Pb . *Earth Planet. Sci. Lett.* 14:442–446.
- KOIDE, M., K. W. BRULAND, and E. D. GOLDBERG. 1973. Th-228/Th-232 and Pb-210 geochronologies in marine and lake sediments. *Geochim. Cosmochim. Acta* 37:1171–1187.
- KRISHNASWAMI, S., D. LAL, J. M. MARTIN, and M. MEYBECK. 1971. Geochronology of lake sediments. *Earth Planet. Sci. Lett.* 11:407–414.
- LARSON, R. E. 1974. Radon profiles over Kilauea, the Hawaiian Islands and Yukon Valley snow cover. *Pure Appl. Geophys.* 112:204–208.
- LAWS, E. A., D. DOLIENTE, J. HIAYAMA, M.-L. HOKAMA, K. KIM, D. LI, S. MINAMI, and C. MORALES. 1993. Hypereutrophication of the Ala Wai Canal, Oahu, Hawaii: Prospects for cleanup. *Pac. Sci.* 47:59–75.
- LI, Y.-H. 1988. Denudation rates of the Hawaiian Islands by rivers and groundwaters. *Pac. Sci.* 42:253–266.
- LI, Y.-H., and S. GREGORY. 1974. Diffusion of ions in sea water and in deep-sea sediments. *Geochim. Cosmochim. Acta* 38:703–714.
- MOBERLY, R., JR. 1963. Rate of denudation in Hawaii. *J. Geol.* 71:371–375.
- NYFFELER, U. P., Y.-H. LI, and P. H. SANTSCHI. 1984. A kinetic approach to describe trace-element distribution between particles and solution in natural aquatic systems. *Geochim. Cosmochim. Acta* 48:1513–1522.
- RESIG, J. M., K. MING, and S. MIYAKE. 1995. Foraminiferal ecology, Ala Wai Canal, Hawai'i. *Pac. Sci.* 49:341–366.
- RITCHIE, J. C., and J. R. MCHENRY. 1990. Application of radioactive fallout cesium-137 for measuring soil erosion and sediment accumulation rates and patterns: A review. *J. Environ. Qual.* 19:215–233.
- ROBBINS, J. A. 1978. Geochemical and geophysical applications of radioactive lead. Pages 285–393 in J. O. Nriagu, ed. *The biogeochemistry of lead in the environment*. Elsevier/North Holland Biomedical Press, Amsterdam.
- . 1985. Great Lakes regional fallout source functions. NOAA Technical Memorandum No. ERL GLERL-56.
- ROBBINS, J. A., and D. N. EDGINGTON. 1975. Determination of recent sedimentation rates in Lake Michigan using Pb-210 and Cs-137. *Geochim. Cosmochim. Acta* 39:285–304.
- SANTSCHI, P. H., Y.-H. LI, D. M. ADLER, M. AMDURER, J. BELL, and U. P. NYFFELER. 1983. The relative mobility of natural (Th, Pb, and Po) and fallout (Pu, Am, Cs) radionuclides in the coastal marine environment: Results from model ecosystem (MERL) and Narragansett Bay. *Geochim. Cosmochim. Acta* 47:201–210.
- SMITH, J. N., and K. M. ELLIS. 1982. Transport mechanism for Pb-210, Cs-137 and Pu fallout radionuclides through fluvial-

- marine systems. *Geochim. Cosmochim. Acta* 46:941–954.
- SMITH, J. N., K. M. ELLIS, and D. M. NELSON. 1987. Time-dependent modeling of fallout radionuclide transport in a drainage basin: Significance of “slow” erosional and “fast” hydrological components. *Chem. Geol.* 63:157–180.
- SNIDVONGS, A., G. M. MCMURTRY, and S. V. SMITH. 1995. ^{210}Pb and ^{137}Cs in sediments and soils of Tomales Bay watershed, northern California. *Geochim. Cosmochim. Acta* (in press).
- SUGAI, S. F. 1990. Transport and sediment accumulation of ^{210}Pb and ^{137}Cs in two southeast Alaskan fjords. *Estuaries* 13:380–392.
- SUGAI, S. F., M. J. ALPERIN, and W. S. REEBURGH. 1994. Episodic deposition and ^{137}Cs immobility in Skarn Bay sediments: A ten-year ^{210}Pb and ^{137}Cs time series. *Mar. Geol.* 116:351–372.
- THOMAS, D. M., K. E. CUFF, and M. E. COX. 1986. The association between ground gas radon variations and geologic activity in Hawaii. *J. Geophys. Res.* 91:12,186–12,198.
- TILLING, R. I., and J. J. DVORAK. 1993. Anatomy of a basaltic volcano. *Nature (Lond.)* 363:125–133.
- TILLING, R. I., C. HELIKER, and T. L. WRIGHT. 1987. Eruptions of Hawaiian volcanoes: Past, present, and future. Department of the Interior, U.S. Geological Survey, Denver, Colorado.
- TORGERSEN, T., and M. E. LONGMORE. 1984. ^{137}Cs diffusion in the highly organic sediment of Hidden Lake, Fraser Island, Queensland. *Aust. J. Mar. Freshwater Res.* 35:537–548.
- TUREKIAN, K. K., Y. NOZAKI, and L. K. BENNINGER. 1977. Geochemistry of atmospheric radon and radon products. *Annu. Rev. Earth Planet. Sci.* 5:227–255.
- U.S. BUREAU OF THE CENSUS. 1991. 1989 estimates. Pages 556–557 in M. S. Hoffman, ed. *The world almanac and book of facts, 1991*. Scripps-Howard Publ., New York.
- U.S. GEOLOGICAL SURVEY. 1967–1990. Water resources data: Hawaii and other Pacific areas. Annual report from 1967 to 1990. U.S. Government Printing Office, Washington, D.C.